Sorbitol Dehydrogenase Overexpression and Other Aspects of Dysregulated Protein Expression in Human Precancerous Colorectal Neoplasms: A Quantitative Proteomics Study*[S]

Anuli Uzozie‡, Paolo Nanni§, Teresa Staiano¶, Jonas Grossmann§, Simon Barkow-Oesterreicher§, Jerry W. Shay‖, Amit Tiwari‡, Federico Buffoli¶, Endre Laczko§, and Giancarlo Marra‡**

Colorectal adenomas are cancer precursor lesions of the large bowel. A multitude of genomic and epigenomic changes have been documented in these preinvasive lesions, but their impact on the protein effectors of biological function has not been comprehensively explored. Using shotgun quantitative MS, we exhaustively investigated the proteome of 30 colorectal adenomas and paired samples of normal mucosa. Total protein extracts were prepared from these tissues (prospectively collected during colonoscopy) and from normal (HCEC) and cancerous (SW480, SW620, Caco2, HT29, CX1) colon epithelial cell lines. Peptides were labeled with isobaric tags (iTRAQ 8-plex), separated via OFFGEL electrophoresis, and analyzed by means of LC-MS/MS. Nonredundant protein families (4325 in tissues, 2017 in cell lines) were identified and quantified. Principal component analysis of the results clearly distinguished adenomas from normal mucosal samples and cancer cell lines from HCEC cells. Two hundred and twelve proteins displayed significant adenoma-related expression changes (q-value < 0.02, mean fold change *versus* normal mucosa ±1.4), which correlated ($r = 0.74$) with similar changes previously identified by our group at the transcriptome level. Fifty-one (~25%) proteins displayed directionally similar expression changes in colorectal cancer cells (*versus* HCEC cells) and were therefore attributed to the epithelial component of adenomas. Although benign, adenomas already exhibited cancer-associated proteomic changes: 69 (91%) of the 76 protein up-regulations identified in these lesions have already been reported in cancers. One of the most striking changes involved sorbitol dehydrogenase, a key enzyme in the polyol pathway. Validation studies revealed dramatically increased sorbitol dehydrogenase concentrations and activity in adenomas and cancer cell lines, along with important changes in the expression of other enzymes in the same (AKR1B1) and related (KHK) pathways. Dysregulated polyol metabolism might represent a novel facet of metabolome remodeling associated with tumorigenesis. *Molecular & Cellular Proteomics 13: 10.1074/mcp.M113.035105, 1198–1218, 2014.*

Colorectal cancer ranks third among the world's high-incidence cancers and is a leading cause of cancer-related death among older adults (1, 2). In the United States alone, projections for 2013 include 102,480 new cases and 50,830 deaths (2). Cancerogenesis in the large bowel begins with the transformation of the epithelial cell lining of the gut. Molecular alterations, mainly involving the WNT signaling pathway, render these cells hyperproliferative, and they form benign adenomatous tumors. The neoplasms are initially noninvasive (3, 4), and the vast majority remain that way. But as genetic and epigenetic anomalies continue to accumulate, the tumor cells' capacity for invasion and destruction of surrounding tissues increases. At some point, this process drives certain adenomas into the realm of frank malignancy, transforming them into adenocarcinomas.

Early diagnosis of colorectal tumors has been greatly facilitated by screening methods based on fecal analysis or colonoscopy, but both approaches have limitations (5–9). Better understanding of the molecular mechanisms underlying large bowel tumorigenesis could improve our chances of detecting these lesions in the adenomatous or localized adenocarcinomatous stage, when the chances of successful treatment are greater. Promising results for the detection and validation of potential cancer biomarkers are emerging from proteomic studies of cancer development (10). Relative to

From the ‡Institute of Molecular Cancer Research, University of Zurich, Zurich 8057, Switzerland; §Functional Genomics Center of the University of Zurich and ETH, Zurich 8057, Switzerland; ¶Gastroenterology and Endoscopy Unit, Hospital of Cremona, Cremona 26100, Italy; ‖University of Texas Southwestern Medical Center at Dallas, Dallas, Texas 75211

Received October 15, 2013, and in revised form, February 7, 2014
Published, MCP Papers in Press, February 24, 2014, DOI 10.1074/mcp.M113.035105

Author contributions: P.N. and G.M. designed research; A.U., P.N., A.T., and E.L. performed research; J.W.S. contributed new reagents or analytic tools; J.G., S.B., and E.L. analyzed data; A.U. and G.M. wrote the paper; T.S. and F.B. performed tissue sample and clinical data collection.

older gel-electrophoresis-based approaches, shotgun proteomics methods, particularly those that include pre-MS OFFGEL electrophoretic peptide fractionation (11), enhance the sensitivity, robustness, and reproducibility of these studies (12) and expand the proteome coverage to include proteins that are less abundantly expressed (13–16). Furthermore, with the aid of isobaric-tag peptide-labeling strategies, MS can also be used for the relative quantification of protein expression levels within a series of multiple human tissue samples (12, 17–19).

Thus far, only a few MS-based proteomics studies have examined human colorectal adenomas (reviewed in Refs. 9 and 20). We therefore decided to explore the proteome of a relatively large series of these precancerous lesions (each with a paired sample of normal colon mucosa) using quantitative shotgun MS with the widely used iTRAQ[1] peptide labeling technique (21, 22) and OFFGEL fractionation. Adenoma-related protein expression variations specific to the epithelial compartments of these lesions were identified with a novel approach, which involved comparing the human tissue proteome with that of colon epithelial cell lines. The results of these studies revealed several protein expression changes previously documented only in advanced colorectal cancers. They also disclosed several novel changes with potentially important roles in early-stage large bowel tumorigenesis, including the marked up-regulation of a key enzyme in the polyol pathway.

EXPERIMENTAL PROCEDURES

Human Tissue Samples and Cell Lines—Human colorectal tissues were prospectively collected from patients undergoing colonoscopy in the Istituti Ospitalieri of Cremona, Italy. Approval was obtained from the local ethics committee, and tissues were used in accordance with the Declaration of Helsinki. Each donor provided written informed consent to sample collection, data analysis, and publication of the findings. Progressive numbers were assigned to each patient to protect human confidentiality. The series comprised 30 colorectal adenomas, each with a paired sample of normal mucosa from the same colon segment, >2 cm from the lesion. Tissues were collected endoscopically, promptly frozen in liquid nitrogen, and stored at −80 °C.

Five colorectal cancer cell lines (HT29, Caco2, CX1, SW480, and SW620) were obtained from the Zurich Cancer Network's Cell Line Repository. All had been recently purchased from the American Tissue Culture Collection (Teddington, UK) and were certified as mycoplasma infection free. We cultured Caco2 and CX1 cells in Dulbecco's modified Eagle's medium; HT29 cells in McCoy's medium; and SW480 and SW620 cells in RPMI 1640 medium supplemented with 10% fetal bovine serum, L-glutamine, and 1% penicillin-streptomycin (Sigma, St. Louis, MO). The recently established line of immortalized human colon epithelial cells (HCEC) was obtained from J. W. Shay and grown as described elsewhere (23).

Protein Extraction from Tissues and Cell Lines—For MS studies, frozen tissue samples were quickly weighed and homogenized on ice (1 min of grinding, 1 min on ice, 1 min of grinding) in a Wheaton glass borosilicate grinder containing a solution of 100 mM triethylammonium bicarbonate (Sigma, St Louis, MO), 1X Complete EDTA-free Protease Inhibitor Mixture (Roche, Mannheim, Germany), 1 M urea, 5 mM β-glycerophosphate disodium salt hydrate, 1 mM sodium orthovanadate, and 5 mM sodium fluoride (Sigma). The efficiency of cell lysis was microscopically confirmed. The homogenates were then sonicated with a Bioruptor (Diagenode, Denville, NJ) (high power, five 10-s/10-s on/off cycles) and centrifuged (16,000*g* for 5 min at 4 °C). The supernatant containing the proteins was collected and stored at −80 °C.

Cells (grown to >80% confluence in 15-cm^2 dishes) were washed in PBS, covered with 250 μl of the buffer used for tissue sample homogenization (see above), detached from the dish with a cell scraper, and homogenized (25 passages through a 25-gauge needle). The efficiency of cell lysis was microscopically confirmed. Sonication and centrifugation were repeated as described above, and the protein concentration was determined via Bradford assay. Prior to MS analysis, a 5-μg sample of each protein extract was subjected to one-dimensional gel electrophoresis on a 12% bisacrylamide gel to assess protein integrity and extraction protocol reproducibility. The entire proteomic workflow, from tissue/cell processing to statistical analysis, is summarized in Fig. 1 and described in detail in the next five subsections.

For sorbitol dehydrogenase (SORD) assays (see below), >80% confluent cells were washed in PBS and covered with a solution consisting of 100 mM triethanolamine (Sigma) and 1X Complete EDTA-free Protease Inhibitor Mixture (Roche). (A simple buffer was used to reduce the risk of introducing anti-enzymatic substances into our extract.) Cells were then scraped and homogenized with 25 passages through a 25-gauge needle. Tissue samples were weighed and homogenized in a Wheaton glass borosilicate grinder containing the buffer described above. After centrifugation (16,000 *g*, 4 °C, 5 min), the supernatant was aliquoted and stored at −80 °C. Protein concentration was measured via Bradford assay.

Protein Digestion and iTRAQ 8-plex Labeling—iTRAQ 8-plex experiments were performed to analyze tissue extracts (10 experiments) and cell-line extracts (1 experiment) (Fig. 1). Labeling efficiency and relative quantitation accuracy were assessed with the aid of two reference protein extract mixtures: one for tissue samples (pooled extracts from three normal tissues and three adenomas) and one for cell lines (pooled aliquots of each of the six cell line extracts). Fifty micrograms of protein per sample were used for each iTRAQ channel. Tryptic digestion (10% w/w, sequencing-grade modified trypsin, Promega, Madison, WI) and iTRAQ 8-plex labeling (AB Sciex, Framingham, MA) were performed according to the manufacturers' instructions (2.5-h incubation of samples with iTRAQ labels). For tissue experiments, two iTRAQ labels, 113 and 114, were chosen for the reference mixture, and labels 115/116, 117/118, and 119/121 were used for the three pairs of normal/adenomatous tissues included in each experiment. For the cell line experiment, labels 113 and 114 were used for the reference mixture, and labels 115–121 represented HCEC, HT29, Caco2, CX1, SW480, and SW620 cells, respectively (Fig. 1). After iTRAQ labeling, the samples (for each experiment) were combined, desalted on 500-mg SepPak C18 columns (Millipore, Billerica, MA), dried in a SpeedVac concentrator (Thermo Scientific), and subjected to peptide fractionation.

OFFGEL Electrophoresis—Peptide fractionation was performed according to the manufacturer's protocols with an Agilent 3100 OFFGEL fractionator and 12-well OFFGEL kit (both from Agilent Technologies, Santa Clara, CA). Briefly, samples were resolubilized in 1.8 ml of 1X OFFGEL peptide stock solution containing carrier ampholytes (pH range 3–10), loaded into the wells (150 μl per well), and focused until 20 kV/h was reached with a maximum current of 50 μA. For each experiment, 12 fractions were collected. A 15-μl aliquot of each fraction was acidified with 1.5 μl of a 50% acetonitrile/1%

[1] The abbreviations used are: iTRAQ, isobaric tags for relative and absolute quantification; HCEC, human colon epithelial cell; FDR, false discovery rate; GO, Gene Ontology; INHAT, inhibitor of acetyltransferases; MS/MS, tandem mass spectrometry; PSM, peptide spectra match; emPAI, exponentially modified protein abundance index; SORD, sorbitol dehydrogenase; TBST, Tris-buffered saline with Tween 20.

trifluoroacetic acid solution, desalted using ZipTip C18 (Millipore, Billerica, MA), dried, resolubilized in 15 μl of a 0.1% formic acid/3% acetonitrile solution, and analyzed with MS.

Liquid Chromatography and Mass Spectrometry—Peptide samples (4 μl) were analyzed on an LTQ-Orbitrap Velos mass spectrometer (Thermo Fischer Scientific, Bremen, Germany) coupled to a nano-HPLC system (Eksigent Technologies, Dublin, CA). The solvent compositions were 0.2% formic acid and 1% acetonitrile for channel A and 0.2% formic acid and 80% acetonitrile for channel B. Peptides were loaded onto an in-house-made tip column (75 μm $\times$ 80 mm) packed with reverse-phase C18 material (AQ, 3 μm, 200 Å, Bischoff GmbH, Leonberg, Germany) and eluted (flow rate, 250 nL/min; solvent B gradient: from 3% to 30% in 62 min, from 30% to 45% in 70 min, and from 45% to 97% in 75 min).

Full-scan MS spectra (300–1700 *m/z*) were acquired at a resolution setting of 30,000 at 400 *m/z* after accumulation to a target value of 1×10^6. For the eight most intense signals per cycle above a threshold of 1000, both collision-induced dissociation and higher-energy collisional dissociation spectra were acquired in a data-dependent manner (Fig. 1). Collision-induced dissociation scans were recorded in the ion trap (settings: normalized collision energy, 35; maximum injection time, 50 ms; automatic gain control, 1×10^4 ions). For the higher-energy collisional dissociation scans, spectra were recorded at a resolution setting of 7500 at 400 *m/z* (normalized collision energy, 52; maximum injection time, 125 ms; automatic gain control, 5×10^4 ions). Charge state screening was enabled, and singly charged states were rejected. Precursor masses previously selected for MS/MS were excluded from further selection for 60 s, and the exclusion window was set at 10 ppm. The maximum number of entries in the exclusion list was set at 500. All samples were analyzed in duplicate, and precursors selected in the first run were excluded from fragmentation in the second run. The exclusion list was set on a time window of 4 min and a mass width of 10 ppm. Spectra were acquired using internal lock mass calibration on *m/z* 429.088735 and 445.120025.

Peak List Generation and Database Search—As depicted in Fig. 1, Mascot Distiller 2.4.3.3 (Matrix Science, Boston, MA) was used to generate Mascot generic format peak lists. De-isotoping and peak picking were not performed between 112.5 and 121.5 *m/z* (the range containing iTRAQ reporter ions), and the higher-energy collisional dissociation and collision-induced dissociation spectra were merged by summing. For each of the 11 experiments, the corresponding 24 Mascot generic format peak lists were concatenated and searched, with the aid of Mascot Server 2.3.02 (Matrix Science), against a forward UniProtKB/Swiss-Prot database for human proteins concatenated to a reversed decoyed FASTA database. The concatenated database contained a total of 147,438 proteins with accessions in Gene Ontology–compatible format and 260 common MS contaminants (NCBI taxonomy I.D. 9606, released December 13, 2011).

Methylthio (C), iTRAQ 8-plex labeling at the N terminus and lysine were set as fixed modifications, and variable modifications consisted of methionine oxidation and iTRAQ 8-plex labeling of tyrosine. We used the iTRAQ 8-plex-vs114 (Applied Biosystems Zug, Switzerland) quantitation method. The isotope and impurity correction factors used for each iTRAQ label were those provided by the manufacturer. Precursor and fragment tolerances were set at 10 ppm and 0.8 Da, respectively. The enzyme specificity was set to trypsin with an allowance of up to one missed cleavage. Using Mascot internal export scripts, we transformed Mascot DAT files into XML files and parsed them with in-house scripts so that peptide sequences, scores, and intensities of the individual reporter ion channels were reported. Confidently identified and quantified peptides were selected with the following filters: rank 1 (best spectra assignment); ion score, > 15; and presence of iTRAQ intensity values for reporter channels 113 and 114.

Quantification of Relative Protein Abundance—(These steps are described in the boxes of the lower half of Fig. 1.) Peptide reporter channel intensities were summed for each protein individually using R-scripts. Ratios were built from summed channels (113/114 to 121/114) for all proteins identified in each iTRAQ experiment. False discovery rates (FDRs) (24) were determined at the spectrum, peptide, and protein levels. The results of individual experiments were then merged into one matrix, which was used for statistical analysis in R and Perseus (Version 1.2.7.4). All proteins identified with the same peptide(s) were grouped into families, each of which was identified by a unique protein family number. Ratios of the intensity of each ion channel to that of 114 were converted to base 2 logarithmic values and normalized respectively on the median (which was set at 0), resulting in ratios that followed a Gaussian distribution. Proteins identified on the basis of the same peptide(s) shared the same family number and were represented once in our statistical analysis. The paired *t* test was used to compare the expression of a given protein in each adenoma and that found in the corresponding sample of normal mucosa. To correct for multiple comparisons, the FDR was controlled with the Benjamini–Hochberg procedure. The average protein-expression fold change in adenomas, relative to the normal mucosa, was then calculated. For this, median normalized ratios for all proteins in each paired adenoma–normal mucosa sample were deconvoluted of the reference standard effects (114) to compute the adenoma *versus* normal mucosa ratio per protein (deconvoluted fold change, $(116/114)/(115/114) = (116/115)$) and the mean fold change per protein in all tissue pairs. The Mascot emPAI values for all proteins were included in XML exports for each experiment. Thereafter, the mean Mascot emPAI value was calculated for all proteins.

Functional Annotation of Proteins—Gene Ontology (GO) annotations and GO terms for proteins in the UniProt/Swiss-Prot database were sourced from the European Bioinformatics Institute. The Scaffold program (Version 3) was used to identify the cellular localizations and biological processes most represented in lists of proteins quantified in tissues and cell lines. The topGO Bioconductor software package in R was used to identify and screen for GO biological process categories displaying enrichment for proteins that were differentially regulated in adenomas (*versus* normal mucosa) (25). First, we prepared a "universe" comprising all the proteins quantified in our study, each matched to GO terms and annotations. This served as the "background." The "foreground" consisted of the list of significantly dysregulated proteins. The most significant GO terms were scored with the Eliminating Genes (*elim*) method (25).

Western Blotting—Proteins were separated on a 10% SDS-polyacrylamide gel and transferred to a hydrophobic polyvinylidene difluoride membrane (GE Healthcare, Amersham Biosciences Hybond-P PVDF membrane, Pittsburgh, PA) according to standard protocols (26). After 1 h of blocking with 5% nonfat dry milk in TBS with 1% Tween 20 (milk–TBST), membranes were incubated overnight with the primary antibody (anti-SORD (HPA040260, Sigma); anti-aldose reductase, AKR1B1 (GTX113381, GeneTex, Irvine, CA); anti-ketohexokinase, KHK (GTX109591, GeneTex)) diluted 1:1000 in milk–TBST and washed once with milk–TBST (20 min) and twice with TBST (20 min). After 1 h of incubation in horseradish-peroxidase-conjugated secondary antibody (anti-rabbit IgG, GE Healthcare) diluted 1:5000 in milk–TBST, membranes were washed once with milk (20 min) and twice with TBST (20 min). Enhanced chemiluminescence (Amersham Biosciences, catalog no. RPN2106) was used to detect immunoreactive proteins.

Immunostaining of Cells and Tissues—HT29 and HCEC cells were seeded (3×10^5 per well) on 22-mm $\times$ 22-mm cover slips in six-well plates and grown under standard conditions until cells reached 70% to 80% confluence. Cells were then washed twice with PBS and fixed in ethanol:methanol solution (50:50) for 10 min at room temperature. Fixed cells were permeabilized (10 min with 0.25% Triton X-100),

blocked (30 min in 10% goat serum (X0907, Dako, Glostrup, Denmark)), and incubated with primary antibody (rabbit polyclonal anti-SORD, HPA040260, Sigma, 1:100) for 18 h at 4 °C. After three washes with PBS, the cells were incubated for 1 h with secondary antibody conjugated to polymer-HRP anti-rabbit (Dako, EnVision+ System-HRP, catalog no. K4010). They were then washed three times in PBS and incubated for 15 min in the substrate-chromogen 3,3-diaminobenzidine tetrahydrochloride (Dako, EnVision+ System-HRP, catalog no. K4010). Cells were washed quickly with PBS and mounted on slides (EUKITT, O. Kindler, GmbH, Freiburg, Germany) for light microscopy (Leica Microsystems GmbH, Wetzlar, Germany). Images were examined and recorded with Leica Application Suite (V3.3.0) software.

SORD immunohistochemistry was performed as previously described (27). Tissue sections (normal colon and ileum, colorectal adenomas, and adenocarcinomas) were incubated for 24 h at 4 °C with primary antibody (rabbit polyclonal anti-SORD, HPA040261, Sigma) at a 1:100 dilution.

Measurement of SORD Activity—Total protein was extracted from cell lines and tissues as described above. SORD catalyzes the reversible conversion of D-sorbitol to D-fructose, with β-NADH as a cofactor.

$$\text{D-fructose} + \beta\text{-NADH} \underset{\text{SORD}}{\longleftrightarrow} \text{D-sorbitol} + \beta\text{-NAD} \quad \text{(Eq. 1)}$$

SORD activity was quantified via continuous spectrophotometric rate measurement of the β-NAD formation rate (temperature 25 °C, pH 7.6, A_{340}, light path of 1 cm) in a Cary 50 Scan UV-visible spectrophotometer using the Cary Kinetics Application (both from Varian Inc., Palo Alto, CA) (28). The final reagent concentrations in a 1-ml cuvette were as follows: 78.33 mM triethonolamine, 183 mM D-fructose, 0.21 mM β-NADH, 0.033% (w/v) BSA. The absorbance reading was recorded when the enzyme was added. One unit of enzyme activity was defined as the amount of enzyme required per minute to convert 1.0 μM D-fructose to D-sorbitol at pH 7.6 at 25 °C. A mixture of reagents plus recombinant SORD was used as the positive control; negative controls consisted of the same reagent mixture with no recombinant SORD, with recombinant SORD but no D-fructose, or with recombinant SORD but no β-NADH.

Extraction and Quantification of Intracellular Metabolites by Targeted Gas Chromatography Coupled with MS—Frozen tissue (50 to 100 mg) was homogenized in 250 μl of ice-cold 80% methanol using a glass borosilicate grinder from Wheaton (Rockdale, UK). The homogenate was microscopically examined to ensure that it was cell free, and then it was transferred to Eppendorf vials and left on ice for 15 min to ensure efficient protein precipitation. After centrifugation (15,000*g* for 3 min at 0 °C), the supernatant was snap-frozen and stored at −80 °C, and the protein content of the pellet was determined via the Bradford method.

For gas chromatography coupled with MS (GC-TOF-MS), 10 μl of supernatant was transferred to a 1.5-ml Eppendorf tube, and internal standards ($^{13}C_1$-sorbitol, $^{13}C_1$-fructose, and $^{13}C_1$-glucose; 1.2 pM of each) were added. The samples were then dried overnight in a vacuum centrifuge (Concentrator 5301, Eppendorf AG, Wesseling-Berzdorf, Germany). Methoxyamine hydrochloride and N-methyl-N-(trimethylsilyl)trifluoroecetamide were used as derivatization reagents (29).

The derivatized metabolites and internal standards were subjected to GC-TOF-MS (GC 7890A, Agilent Technologies, Santa Clara, CA; GCT Premier Micromass, Waters, Manchester, UK) with an Rxi-5Sil MS Integra-Guard column (length, 30 m; internal diameter, 0.25 mm) and a film thickness of 0.25 μm (Restek, Bellafonte, PA). One microliter of each derivatized sample was injected in splitless mode on a baffled glass liner and transferred to the capillary column by rapid heating of the liner from 50 °C to 250 °C at a rate of 12 °C/s. For the separation of the metabolites, helium was used at a flow rate of 1 ml/min, and after an initial hold time of 2 min, a temperature gradient from 80 °C to 320 °C (rate = 8 °C/min) was applied. The TOF-MS was set to acquire centroided standard electron ionization mass spectra over a range of 50 to 600 *m/z* at a rate of three spectra per second. The GC-MS transfer line was heated to 280 °C. Dynamic range enhancement was activated. C_6ClF_5 was used as lock mass compound.

The MassLynx and QuanLynx programs (Waters, UK) were used to review and analyze the acquired data. The absolute concentrations of D-sorbitol, α and β D-fructose, and α and β D-glucose were calculated on the basis of the ratio of the intensity of specific fragments originating from the unlabeled compound to that of the added labeled analog (internal standard). These concentrations were used to estimate intracellular levels per milligram of tissue (adenoma *versus* normal mucosa). The relative concentration of lactate was estimated from the ratio of the intensity of specific fragments originating from the unlabeled compound to that of the added $^{13}C_1$-sorbitol (internal standard).

RESULTS

Proteomic Analysis of Human Colorectal Tissues and Colon Cell Lines—We used a quantitative-MS-based discovery strategy to explore the proteome of human colorectal tissues and colon cell lines (normal and neoplastic). The characteristics of the precancerous colorectal lesions are listed in Table I. Protein extracts from these tumors and their paired samples of normal mucosa (60 samples total) were analyzed using iTRAQ LC-MS/MS and the workflow described in Fig. 1. The inclusion of two reference sample mixes allowed us to control for technical variability across the 10 experiments on tissue samples, as the reference sample was analyzed twice in each experiment. OFFGEL electrophoresis was used to obtain highly reproducible, pI-based, in-solution separation of pooled iTRAQ-labeled peptides. Furthermore, for relative quantification of proteins using iTRAQ reporter ions, we adopted a stringent FDR for peptide spectra matches (PSMs), and high-confidence peptides for protein quantification were selected only if the reporter ions (113 and 114) were quantified in the reference sample mix (iTRAQ reporter channels 113 and 114). The dataset generated with this approach was large and complex, but we developed a simplified analytical method that allowed us to work with and merge the large data files generated after MS/MS (Fig. 1). High-resolution MS/MS spectra acquired on the LTQ-Orbitrap Velos spectrometer after duplicate analysis of OFFGEL tissue sample fractions produced a total of 240 raw files (10 experiments, 120 fractions, 2 replicates). A total of 37,184 (FDR = 0.9%) unique tryptic peptides were confidently identified and quantified from 285,929 unique PSMs (FDR = 0.2%) (Table II, supplemental Table S1). Ten thousand four hundred and fifty-two proteins (FDR = 1.5%) were assembled from the quantified peptides. Proteins that were indistinguishable in MS/MS (*i.e.* two or more proteins identified on the basis of the same peptide sequence; see "Experimental Procedures" for details) were represented as a single family. The result was a total of 4325

TABLE I
Characteristics of the precancerous colorectal lesions included in the study

Patient number	Age	Sex	Colon segment involved	Maximum lesion diameter (mm)	Paris classification[a]	Pit pattern classification[b]	Microscopic appearance	Highest degree of dysplasia in the lesion[c]	Number of lesions at study colonoscopy[d]	Number of previously excised lesions
1	77	M	S	25	IIa+IIc	IIIs-IIIL	TA	LGD	1	0
2	73	F	A	25	IIa+IIc	IIIs-IIIL	TA	LGD	1	2
3	59	M	T	30	IIa+IIc	IIIs+IIIL	TA	LGD	1	0
4	73	F	R	50	Is	IV	VA	LGD	1	0
5	74	M	R	40	Is	IV	VA	HGD	2	1
6	77	M	C	25	IIa	IIIL	VA	LGD	1	0
7	80	M	A	40	IIa	IIIL	TVA	LGD	1	1
8	82	M	A	15	IIa	IIIL	VA	LGD	2	0
9	73	F	S	20	Ip	IV	TVA	LGD	1	0
10	70	F	C	25	IIa	IIIL	TVA	LGD	2	0
11	63	M	A	45	Is	IIIL-IV	TVA	LGD	0	0
12	68	M	A	30	IIa+Is	IIIL-IV	TVA	HGD	0	0
13	60	M	D	30	Is	IV-Vi	TVA	HGD	0	0
14	55	M	C	25	IIa+Is	IIIL-IV	SSA	LGD	0	0
15	70	M	A	15	Is	IV	TVA	LGD	7	0
16	85	F	S	25	Is+IIa	IV	TA	LGD	1	1
17	66	M	A	30	IIa	IIIL	TA	HGD	2	0
18	72	M	A	30	Is	IV	TVA	HGD	2	0
19	71	M	S	30	IIa	IIIL	TVA	LGD	2	0
20	59	M	R	60	Is	IV-Vi	TVA	HGD	1	0
21	78	M	A	50	Is	IV-Vi	TA	LGD	1	0
22	75	M	R	25	Is	IV-Vn	TVA	HGD	6	0
23	73	F	D	25	Is	IV	TA	LGD	1	0
24	69	F	R	90	Is+IIa	IV	TVA	LGD	1	0
25	75	M	T	18	IIa	IIIL	TA	LGD	1	0
26	61	M	A	40	Is+IIa	IV	TVA	LGD	20	0
27	76	M	S	30	Is	IV-Vi	TA	HGD	1	0
28	78	F	R	60	IIa+Is	IV	TVA	LGD	1	1
29	89	M	R	30	Is	IV	TA	LGD	3	0
30	75	M	A	50	Is	IV-Vn	TVA	HGD/cancer	7	0

Abbreviations: M, male; F, female; C, cecum; A, ascending colon; T, transverse colon; D, descending colon; S, sigmoid colon; R, rectum; TA, tubular adenoma; TVA, tubulovillous adenoma; VA, villous adenoma; SSA, sessile serrated adenoma; LGD, low-grade dysplasia; HGD, high-grade dysplasia.

[a] Macroscopic appearance of neoplastic lesions was classified according to the Paris Endoscopic Classification of Superficial Neoplastic Lesions (*Gastrointest. Endosc.* 2003;58(Suppl.):S3–S27).

[b] Morphological analysis of colon crypt patterns according to the Kudo classification (82).

[c] Low-grade versus high-grade dysplasia as defined by the World Health Organization classification of tumors of the digestive system at the editorial and consensus conference in Lyon, France, November 6–9, 1999.

[d] This number includes the lesion included in our proteomic study.

nonredundant protein families, two-thirds (2865, 66%) of which were relatively quantified in at least 9 normal mucosa–adenoma pairs, and 1072 (25%) in all 30 pairs (Table II, supplemental Table S1).

To verify the efficiency of iTRAQ protein labeling, we repeated the database search with methylthio (C) set as a fixed modification and iTRAQ 8-plex (N-term), iTRAQ 8-plex (K), iTRAQ 8-plex (Y), and oxidation (M) set as variable modifications. (All other search parameters were unchanged.) The assigned PSMs were filtered, as described in "Experimental Procedures," and the average iTRAQ labeling efficiency achieved in each of the 10 tissue experiments was 96% (supplemental Table S2). To ascertain the efficacy of including a standard sample mix as a reference for normalization, we compared combined Gaussian plots of $\log_2$-protein ratios of normal mucosa or adenoma samples with the respective reference channel per experiment (*e.g.* 115/114 *versus* 113/114 for normal tissues, 116/114 *versus* 113/114 for adenomas; see Fig. 1). The ratios displayed normal distributions in all channels. For the reference channel (113/114), $\log_2$-ratios were largely centered on 0, whereas the distribution of adenoma and normal channel $\log_2$-ratios was broader and not always centered at 0 (data not shown).

Sample complexity is a common problem in the analysis of proteomic data from human colorectal tissues. It stems in part from contamination of the epithelial cell proteome by proteins from stromal cells (which were inevitably present in our specimens, even though the endoscopic tissue sampling procedure we used yielded superficial specimens with consistently high epithelial contents). Microdissection can be utilized to

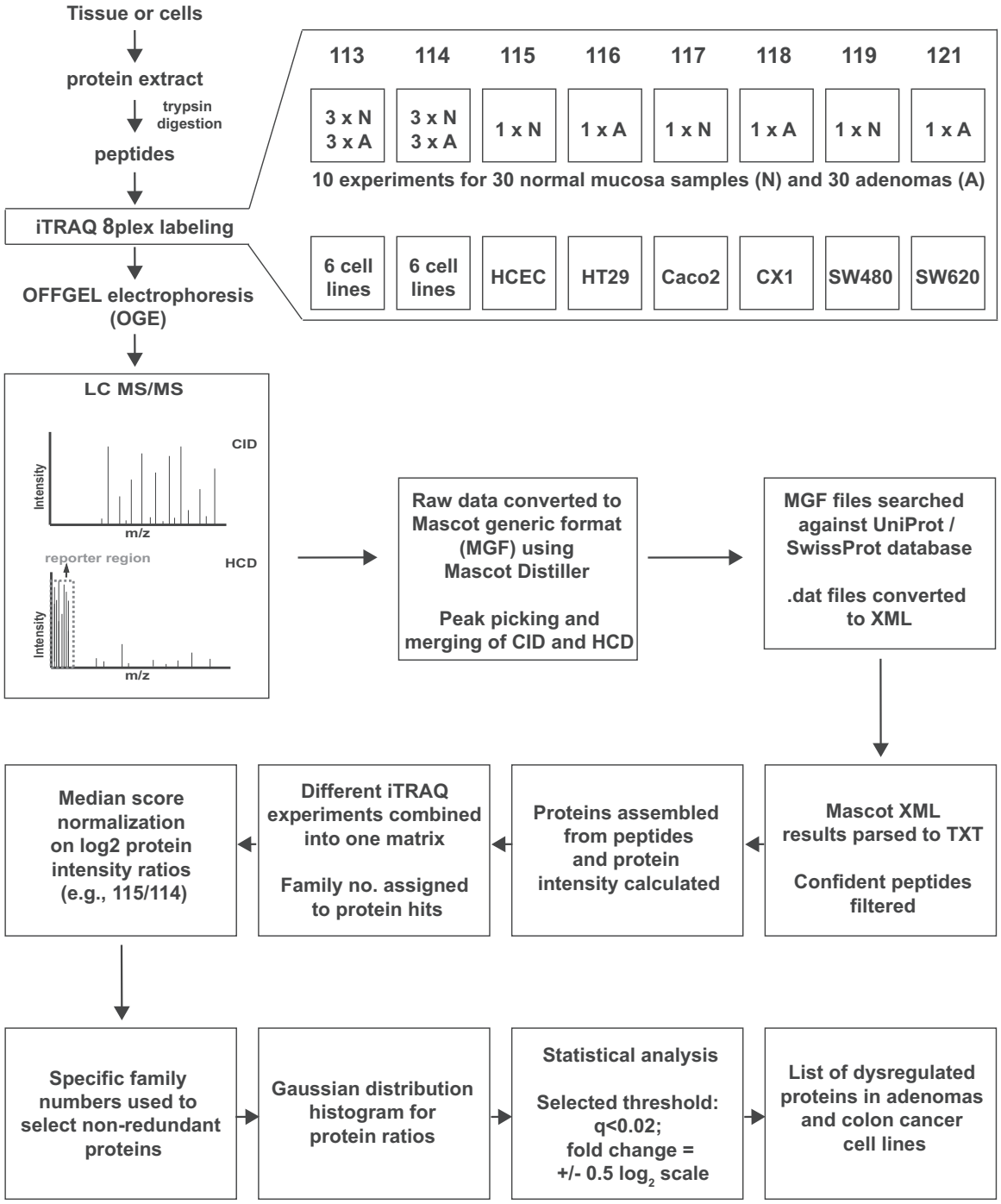

FIG. 1. **Project design and iTRAQ 8-plex labeling scheme.** Sample preparation for shotgun MS/MS and important steps in the analysis of proteomic data for the detection of dysregulated proteins in adenomas and colon cancer cell lines. For each experiment on tissue samples, iTRAQ tags were assigned to a duplicate reference (two identical pools of normal and adenoma samples: 113 and 114, respectively), normal tissues (115, 117, 119) and corresponding adenomas (116, 118, 121). The same pattern was repeated in all 10 experiments. In cell line experiments, two identical pools, each comprising all six cell lines, were used as references (113 and 114), and each of the remaining six tags was used to label a single cell line. The data analysis flow chart depicted in this figure is described in "Experimental Procedures."

isolate subpopulations of cells, but it can diminish the quantity and quality of the proteins, rendering them suboptimal for some types of proteomic analysis. To avoid this problem, we adopted a novel strategy for preliminary identification of the proteomic alterations that were *most likely* to involve the epithelial-cell component of the adenomas. The proteomic profiles of the colon tissues were compared with those of six colon epithelial cell lines (five colon cancer cell lines plus

TABLE II
Summary of proteomics data

	Tissues (n = 60)		Cell lines (n = 6)	
	Total	FDR (%)	Total	FDR (%)
Peptide spectra matches	285,929	0.2	27,922	0.4
Peptides	37,184	0.9	11,266	0.5
Proteins[a]	10,452	1.5	5056	1.1
Proteins[b]	4325	-	2017	-
Proteins[c]	1072	-	1957	-

[a] Total number of proteins quantified in the 10 tissue experiments and the single experiment with cell lines.
[b] Nonredundant protein families quantified in our dataset.
[c] Nonredundant protein families quantified in all 60 tissues or in all six cell lines.

HCEC cells, to our knowledge the only well-characterized line established from normal colorectal epithelium (23)). Changes in expression levels observed in adenomas (*i.e.* up-regulation or down-regulation with respect to normal mucosal levels) were presumed to be epithelial-cell-specific if similar changes were found in the colon cancer cell lines (relative to HCEC cells). After OFFGEL fractionation, duplicate MS analysis of iTRAQ-labeled peptides (24 fractions) from the six cell lines was performed in an LTQ-Orbitrap Velos mass spectrometer, and 11,266 peptides (FDR = 0.5%) were confidently identified and quantified from 27,922 unique PSMs (FDR = 0.4%) (Table II, supplemental Table S3). A total of 2017 nonredundant protein families (FDR = 1.1%) were identified and relatively quantified in cell lines; 1957 (97%) were present in all six cell lines (Table II). In the iTRAQ experiment with cell lines, the peptide labeling efficiency was 95% (supplemental Table S2).

Relative Quantification of the Proteomes of Colorectal Tissues and Cell Lines—The concentration range for proteins expressed in human tissues spans 10 orders of magnitude. We chose not to deplete our protein samples of high-abundance proteins (*e.g.* albumin, IgG), because with the number of tissue samples being analyzed, additional sample preparation steps were considered potential sources of confounding variability (30). As an alternative, each of the 10 pooled iTRAQ-labeled samples (10 experiments) was separated into 12 fractions based on the isoelectric point of peptides, reducing the complexity of our protein matrix and limiting the risk of bias toward the more abundant proteins.

The expression levels of the 4325 nonredundant protein families we were able to relatively quantify in colorectal tissues spanned 4 orders of magnitude, as deduced from the protein Mascot emPAI value (used as a proxy for the emPAI value (31) to estimate protein concentrations) (Fig. 2*A*). Thirty percent (1304/4325) of these families were relatively quantified on the basis of more than one unique peptide. At the top of this list were the large proteins AHNAK, DYNC1H1, DSP, and FCGBP (Fig. 2*B*). In colon epithelial cell lines, 1174 of the 2017 protein families were relatively quantified with more than one unique peptide.

Gene Ontology Annotation in Scaffold was used to identify the subcellular localizations of these protein families and the biological processes they were involved in. The GO categories represented in the tissue and cell line proteomes were fairly similar. In the cell line proteome, however, the categories generally contained fewer proteins, as the total number of proteins detected in these cells was less than that in the tissues (Fig. 2*C*). Cytoplasmic and organelle- or membrane-associated proteins were the most highly represented categories in our extracts, but nuclear proteins were also readily identified, which indicates that our protein extraction procedure was not strongly biased toward a few cell compartments. The most highly represented biological processes in the tissue proteome were metabolic or biosynthetic processes, whereas cell component organization and developmental processes predominated in the cell line proteome (Fig. 2*D*). Stromal contamination was probably responsible for the increased representation of immune system processes in the tissue proteome (relative to that of the cell lines).

Log_2-expression levels of the protein families identified in all tissues (n = 1072) and cell lines (n = 1957) (Table II) were subjected to principal component analysis, which easily distinguished the adenomas from the normal mucosa samples (Fig. 3*A*) and the five colon cancer cell lines from the immortalized normal colon epithelial cell line HCEC (Fig. 3*B*). The cancer cell lines were also segregated into three distinct groups reflecting their patient origins (Fig. 3*B*). When principal component analysis was performed on the expression intensity values of the 1496 nonredundant proteins expressed and quantified in all tissues and cell lines (*i.e.* those representing the intersection of the tissue (n = 10,452) and cell line (n = 5056) protein sets reported in Table II), colon cancer cell lines clustered with adenomas, whereas HCEC cells were closer to the normal mucosa samples (Fig. 3*C*).

As a quality control measure, data for the 60 tissue samples (1072 protein families) were subjected to hierarchical clustering analysis. As shown in supplemental Fig. S1, three main clusters emerged: one consisting almost exclusively of normal mucosa samples, a second containing mainly adenomas, and a third that included both tissue types. The 18 samples in the third cluster (nine adenoma–normal mucosa pairs) formed three subclusters, which corresponded to 3 of the 10 experiments for which trypsin digestion, iTRAQ labeling, and LC-MS/MS were performed on the same day. These findings were suggestive of an experimental bias. Indeed, when these 18 potentially substandard samples were included in subsequent statistical analyses, they diminished the stringency of our threshold and increased the error margin for false identification. We therefore excluded these samples from the analyses described in the following section.

Proteins Displaying Dysregulated Expression in Colorectal Adenomas and Colon Cell Lines—To identify proteins with significantly altered expression in adenomas (relative to normal mucosa), we analyzed data on the proteins quantified in

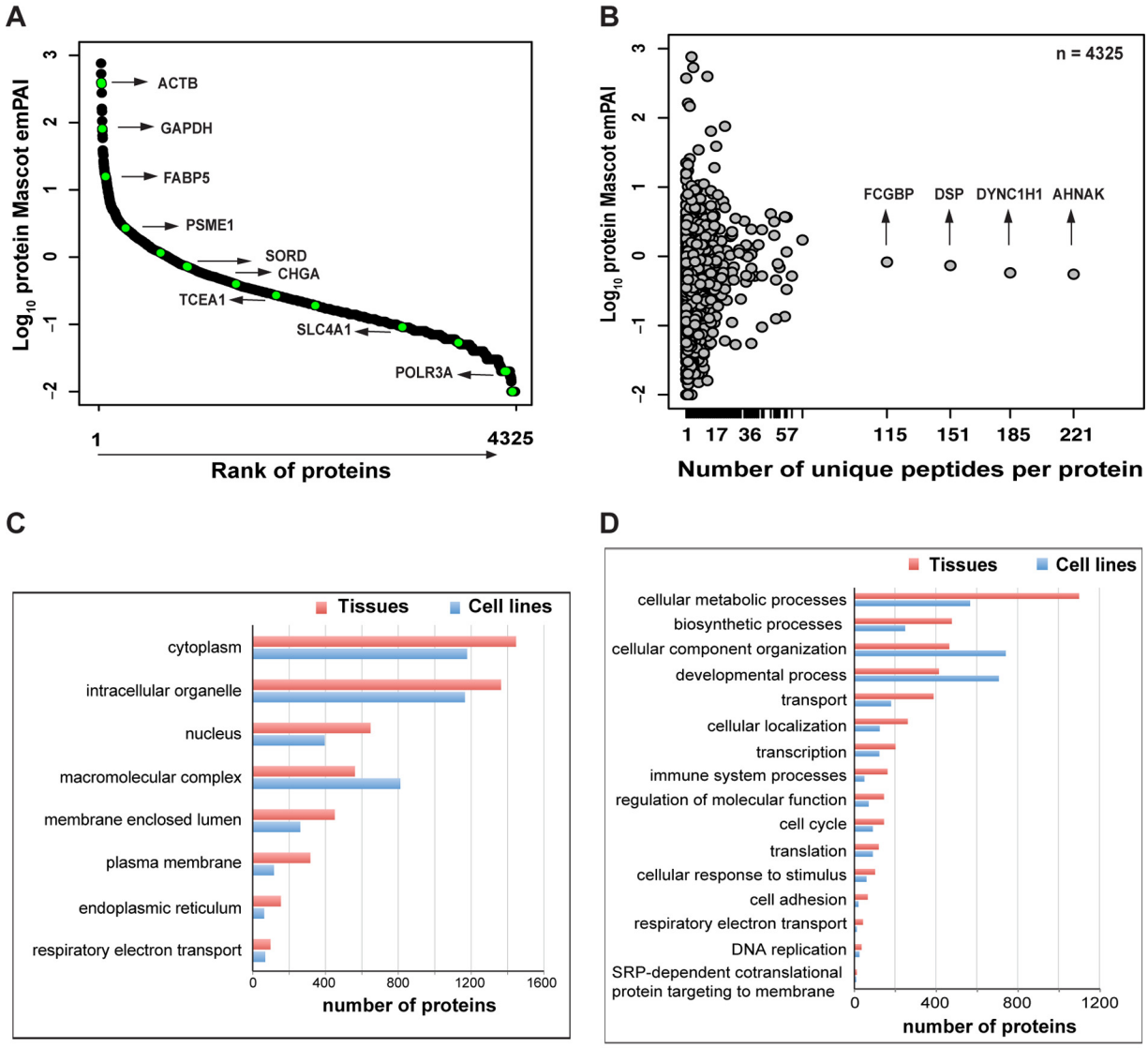

FIG. 2. **Protein coverage with iTRAQ shotgun analysis in colorectal tissues.** *A*, analysis of Mascot emPAI values (used as a proxy for emPAI values) revealed a dynamic range of protein abundance in tissues that spanned 4 orders of magnitude (*y*-axis) and corresponded with known abundance estimates for various proteins in these tissues. The high/moderate-abundance proteins (*e.g.* ACTB, FABP5, CHGA) and low-abundance protein (*e.g.* POLR3A) relatively quantified in our samples are highlighted relative to their mean Mascot emPAI value. *B*, distribution of reported abundance ranges for the proteins with at least one unique peptide identified in tissues, and the high-molecular-weight proteins with the greatest number of unique peptides identified. Subcellular localizations of the proteins identified in colorectal tissues and cell lines (*C*) and biological processes in which these proteins are involved (*D*). This analysis was performed using Scaffold and Gene Ontology annotations (see "Experimental Procedures").

the remaining 21 tissue pairs. The experimentally derived protein fold-change threshold defining differential expression was based on comparison of the distributions of average intensity $\log_2$ ratios in the reference standard (113 *versus* 114, seven experiments) and in patient samples (adenoma *versus* normal, seven experiments). The average ratios in the reference sample were centered on 1 (*i.e.* $\log_2$ 0). Average fold-change ratios for the tissue samples displayed wider variance (supplemental Fig. S2). Seventeen percent of the $\log_2$ ratios for the tissue samples exceeded $\pm$0.5 $\log_2$ scale (indicating a linear fold change $\geq \pm$1.4), as opposed to only 5% of those for the reference samples. For each protein, a paired *t* test was used to compare the intensity ratios in normal and adenomatous samples (*i.e.* normal/114; adenoma/114). After adjustment for multiple comparison (Benjamini–Hochberg method), we selected a stringent q value cutoff of $\leq$0.02.

The 212 proteins that satisfied this criterion and presented a mean expression fold change of $\pm$1.4 ($\log_2$ 0.5) or greater were classified as significantly dysregulated in adenomas. They included 76 with up-regulated expression and 136 with down-regulated expression in the tumor samples (Table III). When protein abundance iTRAQ ratios for these 212 proteins

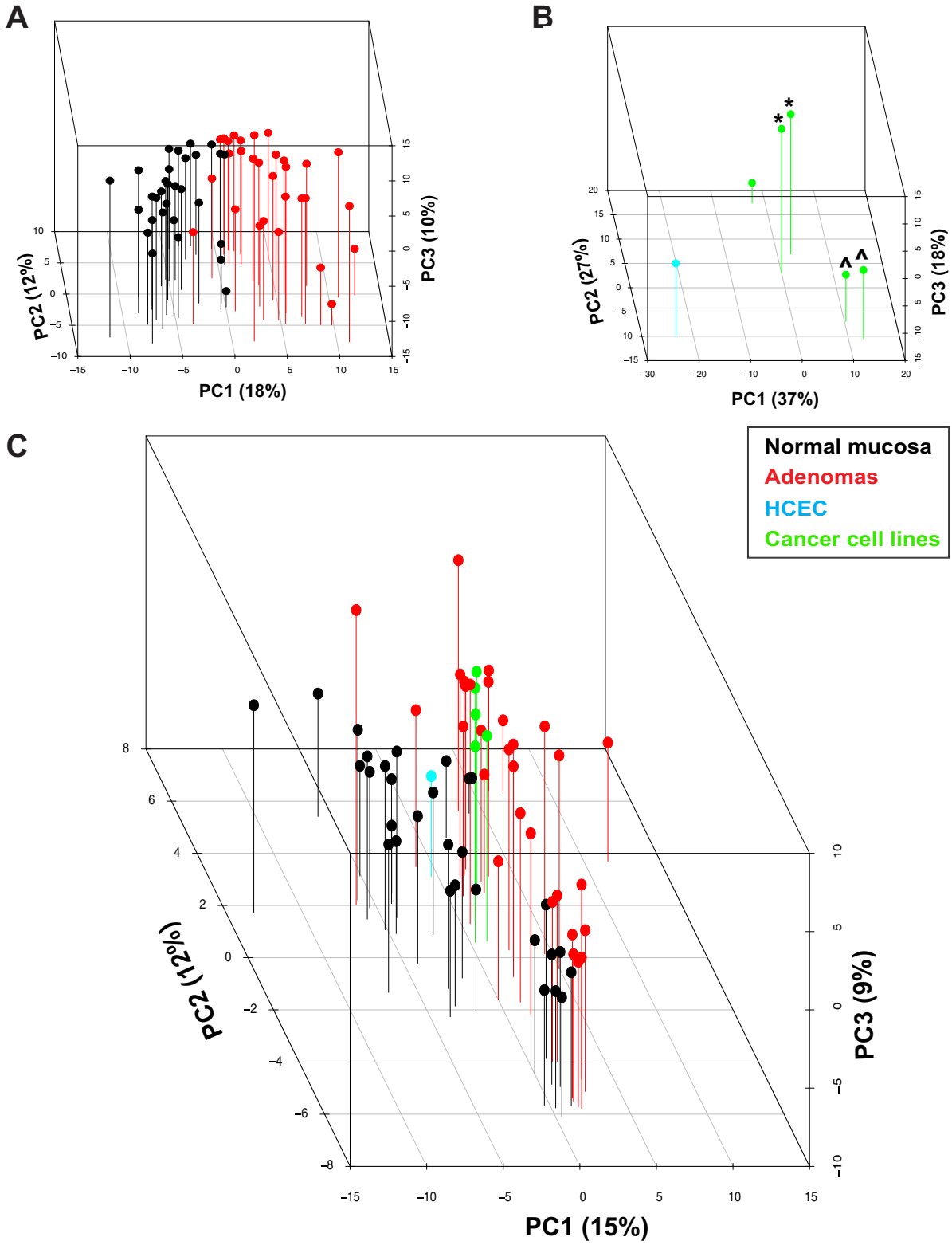

FIG. 3. **Principal component analysis of protein expression.** Three-dimensional principal component analysis score plot of log2 protein expression intensity values for (*A*) tissues (normal mucosa, black; adenomas, red), (*B*) cell lines (HCEC, cyan; colon cancer cell lines, green), and (*C*) both. The first three principal components (PCs) account for 40%, 82%, and 36% of the total variance in the tissue, cell line, and tissue + cell line sets, respectively. PC1, the main direction of spread in the three groupings, reflects intergroup variance based on tissue or cell line type (*i.e.* normal/immortalized *versus* tumorous). Cell lines derived from the same patient: *SW480 and SW620 cells; ^HT29 and CX1 cells.

TABLE III
Proteins displaying differential expression in adenomas versus normal mucosa

UniProt accession number[a]	Gene name	q value	Average fold change (log2)
P12429	ANXA3	0.00000001	1.44
Q9UN36	NDRG2	0.00000001	−0.79
P00918	CA2	0.00000003	−2.26
P23946	CMA1	0.00000005	−1.38
P00488	F13A1	0.00000005	−1.30
Q9UBR2	CTSZ	0.00000016	−1.23
P10645	CHGA	0.00000016	−1.82
O60844	ZG16	0.00000024	−2.02
P17174	GOT1	0.00000045	−0.61
P31949	S100A11	0.00000062	1.49
P00338[b]; **P07195**	LDHA; LDHB	0.00000068	0.62
O60701	UGDH	0.00000104	−0.70
P55011	SLC12A2	0.00000115	0.85
O95571	ETHE1	0.00000120	−0.74
Q01105	SET	0.00000230	0.72
Q16851	UGP2	0.00000275	−0.53
Q00796	SORD	0.00000275	0.62
P20231; Q15661	TPSB2; TPSAB1	0.00000275	−1.51
Q15181; **Q9H2U2**[b]	PPA1; PPA2	0.00000421	0.64
Q9H3G5	CPVL	0.00000467	−0.69
P01282	VIP	0.00000722	−1.10
P07339	CTSD	0.00000856	−0.71
P19338	NCL	0.00000934	0.50
Q6UWP2	DHRS11	0.00001070	−1.20
P04066	FUCA1	0.00001240	−1.32
Q53EL6	PDCD4	0.00001270	−0.51
P07585	DCN	0.00001580	−1.36
P02511	CRYAB	0.00002720	−1.19
Q96CX2	KCTD12	0.00003590	−0.70
Q05707; **P08123**	COL14A1	0.00004020	−1.21
P51884	LUM	0.00004160	−0.96
Q15063	POSTN	0.00004240	−2.10
P21397	MAOA	0.00004240	−0.63
O00748	CES2	0.00004610	−0.88
Q56VL3	OCIAD2	0.00004960	0.95
Q9BYZ8	REG4	0.00004960	0.98
P55008	AIF1	0.00005650	−0.75
P50224; **P50225**	SULT1A3; SULT1A1	0.00005760	−0.63
O14773	TPP1	0.00006430	−0.52
Q16853	AOC3	0.00006650	−1.16
P53634	CTSC	0.00006940	−0.58
O95881	TXNDC12	0.00006940	0.55
O75795	UGT2B17	0.00006940	−1.57
O00391	QSOX1	0.00006940	−0.70
Q99538	LGMN	0.00006940	−0.63
P12111	COL6A3	0.00006990	−0.74
P80188	LCN2	0.00006990	1.32
P12956[b]	XRCC6	0.00007190	0.53
Q6NZI2	PTRF	0.00007860	−0.76
P09382	LGALS1	0.00007880	−0.84
P25815	S100P	0.00008020	3.38
Q15118	PDK1	0.00008120	−0.90
O75380	NDUFS6	0.00008650	−0.63
Q9HAW8	UGT1A10	0.00009090	−0.95
P01042	KNG1	0.00009660	−0.74
O75356	ENTPD5	0.00012385	−0.54
Q15293	RCN1	0.00012867	0.61
P17931	LGALS3	0.00013151	−0.62
P36952	SERPINB5	0.00013151	1.31

TABLE III—*continued*

UniProt accession number[a]	Gene name	q value	Average fold change (log2)
P09211[b]	GSTP1	0.00014809	0.55
P20774	OGN	0.00015467	−1.52
Q8NBJ4	GOLM1	0.00015467	−0.51
Q16563	SYPL1	0.00015568	1.16
P04229; P13761; Q30134; Q9TQE0; Q9GIY3; Q29974; P04440; P79483	HLA-DRB1; HLA-DRB1; HLA-DRB1; HLA-DRB1; HLA-DRB1; HLA-DRB1; HLA-DPB1; HLA-DRB3	0.00015568	−0.81
P35555	FBN1	0.00017230	−0.74
Q9H4M9; **Q9NZN4**; **Q9H223**	EHD1; EHD2; EHD4	0.00017230	−0.56
O00754	MAN2B1	0.00017278	−0.65
B4DR31	DPYSL2	0.00018023	−0.55
P06703[b]	S100A6	0.00018025	1.18
P19801	ABP1	0.00022289	−0.50
P20042	EIF2S2	0.00022417	0.68
P51858	HDGF	0.00024151	0.56
P49959[b]	MRE11A	0.00024174	0.64
O00299[b]; **Q9Y696**	CLIC1; CLIC4	0.00024726	0.67
P61604[b]	HSPE1	0.00024977	0.52
O43252; O95340	PAPSS1; PAPSS2	0.00027464	−0.57
Q12765	SCRN1	0.00029349	−0.64
Q9HB40	SCPEP1	0.00030328	−0.87
P48556	PSMD8	0.00032019	0.56
O60547	GMDS	0.00034711	0.58
Q9Y6R7	FCGBP	0.00035167	−0.73
P61626	LYZ	0.00036558	0.74
Q9Y224	C14orf166	0.00038868	0.52
P01765; P01764	(Ig heavy chain V-III region TIL; Ig heavy chain V-III region VH26)	0.00038868	−0.69
Q9NVP1	DDX18	0.00038996	0.67
P80365	HSD11B2	0.00039413	−0.68
P39687; **Q92688**	ANP32A; ANP32B	0.00039654	0.56
Q86WA6	BPHL	0.00046215	0.52
P24298	GPT	0.00047338	−0.56
Q12874	SF3A3	0.00052166	0.50
P04899; **Q14344**; **P63092**	GNAI2; GNA13; GNAS	0.00062192	−0.51
Q15124	PGM5	0.00068593	−0.68
Q9HAW7; **Q9HAW9**; **O60656**	UGT1A7; UGT1A8; UGT1A9	0.00071202	−0.87
P19224	UGT1A6	0.00071202	−0.87
P06748	NPM1	0.00071508	0.81
Q9NUV9	GIMAP4	0.00071508	−0.89
P18283[b]	GPX2	0.00071508	0.54
P13688	CEACAM1	0.00072482	−1.06
P01591	IGJ	0.00084082	−1.10
P19823	ITIH2	0.00085565	−0.71
P01774; P01776; P01779	(Ig heavy chain V-III region POM; Ig heavy chain V-III region WAS; Ig heavy chain V-III region TUR)	0.00085565	−0.79
P27695[b]	APEX1	0.00086971	0.54
Q9C002	NMES1	0.00087016	−0.91
Q96F85	CNRIP1	0.00088956	−1.27
Q9BPX5	ARPC5L	0.00095098	0.67
P62263	RPS14	0.00095182	0.52
Q9BY32	ITPA	0.00095634	0.51
P01625	(Ig kappa chain V-IV region Len)	0.00097041	−0.61
Q15582	TGFBI	0.00097041	0.90
Q07021[b]	C1QBP	0.00101874	0.76
P00738	HP	0.00102030	−0.61
O15143	ARPC1B	0.00103757	−0.50
Q03154	ACY1	0.00108571	0.60
Q9HCB6	SPON1	0.00115609	−0.89
Q96HE7	ERO1L	0.00119027	0.50
P08575	PTPRC	0.00119950	−0.52

TABLE III—*continued*

UniProt accession number[a]	Gene name	q value	Average fold change (log2)
Q9Y266	NUDC	0.00152358	0.56
P63313; P62328	TMSB10; TMSB4X	0.00159602	0.98
Q96SQ9	CYP2S1	0.00162405	0.84
Q71U36	TUBA1A	0.00162405	0.54
P00915	CA1	0.00163258	−1.18
P04844	RPN2	0.00165748	0.55
P09669	COX6C	0.00171230	−0.61
P21980	TGM2	0.00174251	−0.55
P00325	ADH1B	0.00175658	−1.18
O14745	SLC9A3R1	0.00175658	−0.51
Q9H8H3	METTL7A	0.00179938	−0.50
P61009	SPCS3	0.00186488	−0.69
Q15746; O15264; Q16539	MYLK; MAPK13; MAPK14	0.00186488	−0.53
P01876; P01877; **Q92973**	IGHA1; IGHA2; TNPO1	0.00191760	−1.01
P12109	COL6A1	0.00194792	−0.67
Q9BX66	SORBS1	0.00205902	−0.64
E9PGJ9	CC2D1A	0.00213982	−0.53
P49006	MARCKSL1	0.00233532	0.51
Q01524	DEFA6	0.00233532	1.60
P01620	(Ig kappa chain V-III region SIE)	0.00238585	−0.56
P36873	PPP1CC	0.00240171	0.58
Q07507	DPT	0.00240576	−1.28
P37840	SNCA	0.00261720	−0.57
P00326; P07327	ADH1C; ADH1A	0.00271753	−1.17
P22105	TNXB	0.00271753	−0.51
O95299	NDUFA10	0.00272901	−0.84
Q9NRP0	OSTC	0.00275806	0.76
P10082	PYY	0.00282902	−1.59
P21810	BGN	0.00283401	−0.66
Q8IV08	PLD3	0.00295758	−0.74
P01857; P01859; P01860; P01861	IGHG1; IGHG2; IGHG3; IGHG4	0.00343621	−0.57
P62330	ARF6	0.00343645	0.84
Q03135	CAV1	0.00346186	−0.71
P22309; P35503; P22310; P35504	UGT1A1; UGT1A3; UGT1A4; UGT1A5	0.00349148	−0.87
Q9NSU2	TREX1	0.00349148	−0.76
Q9UKY7	CDV3	0.00355684	0.79
Q7Z4V5	HDGFRP2	0.00360855	0.65
P07357	C8A	0.00372327	−0.62
Q99757	TXN2	0.00377179	−0.73
P13686	ACP5	0.00385765	−0.80
Q8WWA0	ITLN1	0.00392858	−1.30
P62861	FAU	0.00395014	0.51
P57737	CORO7	0.00401004	−0.83
P10606	COX5B	0.00412793	−0.71
Q9Y259	CHKB	0.00420774	−0.59
Q9Y2J8	PADI2	0.00435864	−0.50
O94919	ENDOD1	0.00451988	−0.80
B9A064; P0CG05; A0M8Q6	IGLL5; IGLC2; IGLC7	0.00451988	−0.56
P20039	HLA-DRB1	0.00459324	−0.82
P63167[b]; **Q96FJ2**	DYNLL1; DYNLL2	0.00468484	0.63
Q9UNN8	PROCR	0.00480932	−0.78
P07099	EPHX1	0.00486543	−0.54
P32322	PYCR1	0.00495977	0.55
Q9P0J0	NDUFA13	0.00534323	−0.60
E7EUF8; **E9PFN5**	EPB41L3; GSTK1	0.00539222	−0.95
O75531	BANF1	0.00560405	0.73
P26447	S100A4	0.00562754	−0.53
Q9NVJ2	ARL8B	0.00562754	0.50
Q8N752	CSNK1A1	0.00562754	0.52
P40616	ARL1	0.00583778	0.60

TABLE III—*continued*

UniProt accession number[a]	Gene name	q value	Average fold change (log2)
Q96GA7	SDSL	0.00583778	−0.82
P01275	GCG	0.00607808	−1.33
P15289	ARSA	0.00633336	−0.57
O75521	ECI2	0.00635218	−0.60
P62158[b]	CALM1; CALM2; CALM3	0.00657472	0.67
P49821	NDUFV1	0.00669319	−0.66
Q15746–5	MYLK	0.00678109	−0.51
Q96BM9	ARL8A	0.00686655	0.54
Q6UX06	OLFM4	0.00696505	1.14
P10153	RNASE2	0.00724902	−0.50
P19075[b]	TSPAN8	0.00837908	0.59
Q8WU39	PACAP	0.00837978	−0.56
P21953	BCKDHB	0.00837978	0.54
O76041	NEBL	0.00837978	0.71
Q9H4G4	GLIPR2	0.00849532	−1.10
P01766; P01767; P01768	(Ig heavy chain V-III region BRO; Ig heavy chain V-III region BUT; Ig heavy chain V-III region CAM)	0.00895132	−0.61
Q9NR56; Q5VZF2	MBNL1; MBNL2	0.00996176	0.55
P27105	STOM	0.01083127	−0.51
P05387	RPLP2	0.01100903	0.62
Q96AB3	ISOC2	0.01164408	−0.51
O43294	TGFB1I1	0.01198321	−0.57
Q08752	PPID	0.01211602	0.55
Q96DG6	CMBL	0.01289211	−0.51
P61619	SEC61A1	0.01375705	0.59
P56381; **Q5VTU8**	ATP5E; ATP5EP2	0.01440856	−0.52
P14174[b]	MIF	0.01488262	0.51
P12110	COL6A2	0.01526347	−0.53
Q14956	GPNMB	0.01546825	−0.63
P46952	HAAO	0.01570996	−0.53
Q86VN1	VPS36	0.01610077	0.67
Q96S52	PIGS	0.01626862	−0.61
P15559[b]	NQO1	0.01626862	0.56
O60575	SPINK4	0.01810104	0.77
P55735	SEC13	0.01827155	0.59
P02452	COL1A1	0.01933726	−1.32
P00403	MT-CO_2	0.02012815	−0.62

[a] Two or more accession numbers: proteins from the same family or isoforms from the same gene. Boldface numbers indicate "epithelial cell signature" proteins (see text).

[b] Designated candidate cancer biomarkers in the Human Protein Atlas database.

were plotted on a heat map, adenomas and normal mucosa samples formed two distinct clusters (Fig. 4*A*). As shown in Fig. 4*B*, tissue expression levels for the 212 dysregulated proteins showed good correlation ($r = 0.74$, $p < 0.001$, 95% confidence interval = 0.67–0.79) with those of mRNAs for the same genes (measured by our group in another set of colorectal adenomas) (26).

Table IV lists the biological processes that were overrepresented in this set of proteins. At the top of this list was xenobiotic metabolism, a process already linked with adenoma formation on the basis of enrichment studies of transcriptomic datasets conducted by our group (32). Three of the dysregulated proteins involved in this process (CYP2S1, NQO1, and GSTP1) displayed up-regulated expression in adenomas, but most were characterized by tumor-related down-regulation (ADH1B, ADH1C/ADH1A, UGT1A9/UGT1A6, UGT1A1/UGT1A4/UGT1A3/UGT1A5, UGT1A7/UGT1A8, UGDH, MAOA, SULT1A3/SULT1A1, PAPSS1/PAPSS2, UGP2). Network-building analysis revealed that all these proteins were linked by subnetworks controlled by cancer-associated transcription factors, such as SP1 or, less frequently, MYC, HIF1A, or TP53 (supplemental Fig. S3). As noted in Table IV, a very similar picture emerged when GO enrichment was also analyzed in a larger set of 621 dysregulated proteins selected with less stringent criteria (q value cutoff ≤ 0.2; average $\log_2$ fold change $\geq \pm 0.5$).

The expression levels of 111 (52%) of the 212 proteins that were differentially expressed in adenomas were also quantified in cell lines (those shown in bold in Table III and referred to hereinafter as the "epithelial cell signature" proteins). Almost half ($n = 51$, 46%) showed directionally similar tumor-related dysregulation in both analyses. Because cell line stud-

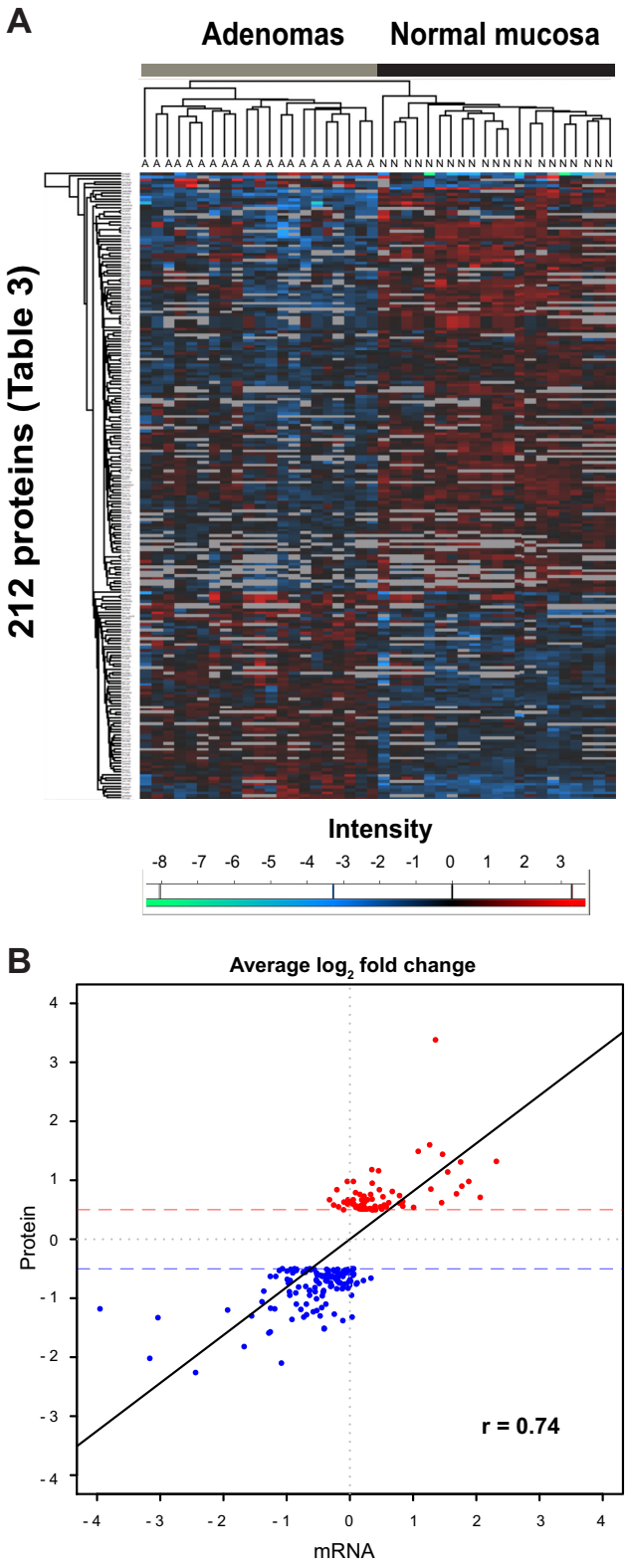

FIG. 4. **Analysis of the 212 proteins displaying significant tumor-related dysregulation.** *A*, hierarchical clustering of iTRAQ abundance ratios (normal *versus* 114, adenoma *versus* 114) for the 212 proteins displaying significant adenoma-related dysregulation grouped tissue samples into two discrete clusters: adenoma (A) and normal (N). *B*, Pearson's correlation test comparing average fold changes (at least ± 0.5 $\log_2$) for the 212 proteins (red, up-regulated; blue, down-regulated) in the tissue series with average $\log_2$ fold changes for the corresponding mRNAs measured in another set of adenoma/normal mucosal samples.

ies were conducted with only one noncancerous line, these findings obviously require further validation. They suggest, however, that these 51 proteins are indeed expressed in the epithelial cells of normal colorectal tissues and that their expression is dysregulated in the epithelial cells of adenomas.

Up-regulation of SORD Expression and Activity in Colorectal Adenomas and Cancer Cell Lines—Sorbitol dehydrogenase, a key enzyme in the polyol pathway, was one of the most significantly up-regulated proteins in our colorectal adenomas (based on q values) (Table III). Because its increased expression could have metabolic consequences with potential effects on tumorigenesis, we performed Western blotting and immunostaining studies to validate this finding. The reliability of the anti-SORD antibody we had chosen was first tested on protein extracts from the six colorectal epithelial cell lines (Fig. 5*A*). The tumor-related $\log_2$ fold changes detected with Western blotting were substantially greater than those documented with iTRAQ (2 to 6 *versus* 0.4 to 1, respectively) (Fig. 5*B*), which was not surprising, as iTRAQ has been reported to underestimate protein abundance (33). However, the relative quantities of SORD found with the two methods were fully consistent. As for the 21 adenomas, the elevated SORD expression documented in these tumors by iTRAQ (Fig. 5*C*) showed good correlation with the increased *SORD* mRNA levels we had previously found in 42 other lesions of this type (26) (Fig. 5*D*). Western blot analysis of four randomly selected adenoma–normal mucosa pairs from the present series revealed obvious up-regulation of SORD expression in all four tumors, although the magnitude of the increase varied (Fig. 5*E*).

SORD activity was then assayed (see "Experimental Procedures") to see how it corresponded with the enzyme expression levels reported above. As shown in Fig. 5*F*, the results of cell line assays were fully consistent with the Western blotting data: SORD activity was seven times higher in HT29 than in HCEC cells, and more limited up-regulation was found in SW480. High correlation between enzyme activity and protein level was also documented for three randomly selected adenoma–normal mucosa pairs (Fig. 5*F*).

MS and Western blotting findings were further validated with immunostaining studies, as shown in Fig. 6. Cytoplasmic SORD staining was evident in the colon cancer cell line HT29 but was weaker or even absent in normal epithelial HCEC cells (Figs. 6*A* and 6*B*). As for colorectal tissues, SORD cytoplasmic expression was limited to the bottom of the normal epithelial crypts (Figs. 6*C*, 6*D*, and 6*E*), but its expression was markedly increased in adenomatous and cancerous glands (Figs. 6*F*–6*I*). These findings suggest that SORD is likely to be

TABLE IV
Gene Ontology (GO) biological processes enriched in the set of 212 proteins whose expression displayed adenoma-related dysregulation (see Table III)

GO I.D.	GO term	Annotated[a]	Significant[b]	Up in adenomas	Down in adenomas	Expected[c]	*elim p* value[d]
GO:0006805	Xenobiotic metabolic process[e]	64	21	3	18	2.8	1.70E-09
GO:0006958	Complement activation, classical pathway[e]	74	17	0	17	3.24	1.10E-08
GO:0051552	Flavone metabolic process[e]	5	5	0	5	0.22	1.50E-07
GO:0052696	Flavonoid glucuronidation[e]	5	5	0	5	0.22	1.50E-07
GO:0052697	Xenobiotic glucuronidation[e]	5	5	0	5	0.22	1.50E-07
GO:0042573	Retinoic acid metabolic process[e]	9	6	0	6	0.39	5.00E-07
GO:0045087	Innate immune response[f]	249	33	4	29	10.91	7.80E-07
GO:0031295	T-cell costimulation[f]	34	10	0	10	1.49	1.10E-06
GO:0030199	Collagen fibril organization[e]	8	5	0	5	0.35	7.80E-06
GO:0001501	Skeletal system development	54	11	1	10	2.37	1.60E-05
GO:0070208	Protein heterotrimerization[e]	5	4	0	4	0.22	1.70E-05
GO:0050852	T-cell receptor signaling pathway[f]	48	10	0	10	2.1	3.20E-05

[a] Proteins in TopGO Background list.
[b] 212 dysregulated proteins of Table III.
[c] Number of significant proteins expected to map to the GO term if the significant proteins are randomly distributed over all GO terms.
[d] *p* value from the Eliminating Genes method (25). Only processes with an *elim p* value $< 1.0E-04$ are shown.
[e] Processes that were also among the top 12 processes displaying enrichment in a larger set of 621 dysregulated proteins selected with less stringent criteria (q value ≤ 0.2; average $\log_2$ fold change $\geq \pm 0.5$; see "Results" section for details).
[f] Processes that shared a common GO ancestor (immune system process) with the process displaying the most significant enrichment in the larger set.

expressed in proliferating cells, although it was largely absent in HCECs, which undergo regular proliferation *in vitro*. Furthermore, nuclear localization of SORD was noted in some adenomatous crypts (supplemental Figs. S4*A* and S4*C*), and the cells in question were almost always negative for the well-known proliferation marker Ki-67 (supplemental Figs. S4*B* and S4*D*). This mutually exclusive staining pattern was also observed in normal crypts of the ileum, where SORD, interestingly, appeared to be expressed in the nuclei of putative stem cells (supplemental Figs. S4*E* and S4*F*).

Polyol Pathway Enzyme Expression and Metabolite Levels in Cell Lines and Tissues—We then examined the state of the polyol pathway (supplemental Fig. S5*A*) in colorectal cell lines and tissues. As shown in supplemental Fig. S5*B*, immunoblot studies revealed decreased AKR1B1 expression in HT29 (*versus* HCEC cells) and adenomas (*versus* corresponding normal mucosal samples), whereas SORD expression and that of KHK were up-regulated in tumor cells and tissues. As for the metabolites (supplemental Fig. S5*C*), D-glucose levels were significantly decreased in adenomas. Less dramatic changes were observed in the levels of D-sorbitol and D-fructose, which both showed a tendency to decrease in tumor tissues.

DISCUSSION

Although a number of proteomic studies have comparatively analyzed different types of colorectal tissues, precancerous lesions have been considered in only three (21, 34, 35), and in two of these (21, 34), the number of adenomas analyzed was very small (≤4). The study by Lam *et al.* (35) is the only one that compared protein expression in a relatively large number ($n = 20$) of paired adenoma and normal mucosa samples. They used two-dimensional gel electrophoresis to resolve over 1000 proteins in the two tissue groups, and those displaying differential expression were then analyzed with MALDI-TOF/TOF-MS. MS/MS validation pinpointed four proteins (ANXA3, S100A11, EIF-5A1, and S100P) whose expression in adenomas was significantly increased. Using MS with iTRAQ 8-plex peptide labeling and OFFGEL fractionation allowed us to quantitatively compare protein expression in 30 colorectal adenomas and paired samples of normal mucosa and investigate low-abundance proteins that cannot be evaluated with proteomics based on two-dimensional gel electrophoresis. All in all, 4325 nonredundant protein families were quantified in our colorectal tissues (25% of which were identified in all 60 samples) (Table II), and the 212 proteins we flagged as significantly dysregulated in adenomas included three of the four proteins identified by Lam *et al.* (up-regulation of the fourth, EIF-5A1, failed to meet our stringent criterion for significance) (Table III).

The cell types in which these proteomic changes occur is of obvious interest, as colorectal cancer arises from the epithelial component of the colorectal mucosa. Although our findings are preliminary and will naturally require validation in future studies, 51 of the 212 proteins listed in Table III were "epithelial cell signature" proteins and showed directionally similar expression changes in colon cancer cell lines *versus* HCEC. It therefore seems likely that their dysregulated expression in adenomas is a feature of neoplastic transformation of colorectal epithelial cells. However, epithelial–stromal cell interactions can also play important roles in tumorigenesis (20). Our approach also allowed us to identify 101 proteins displaying adenoma-related dysregulation that were probably

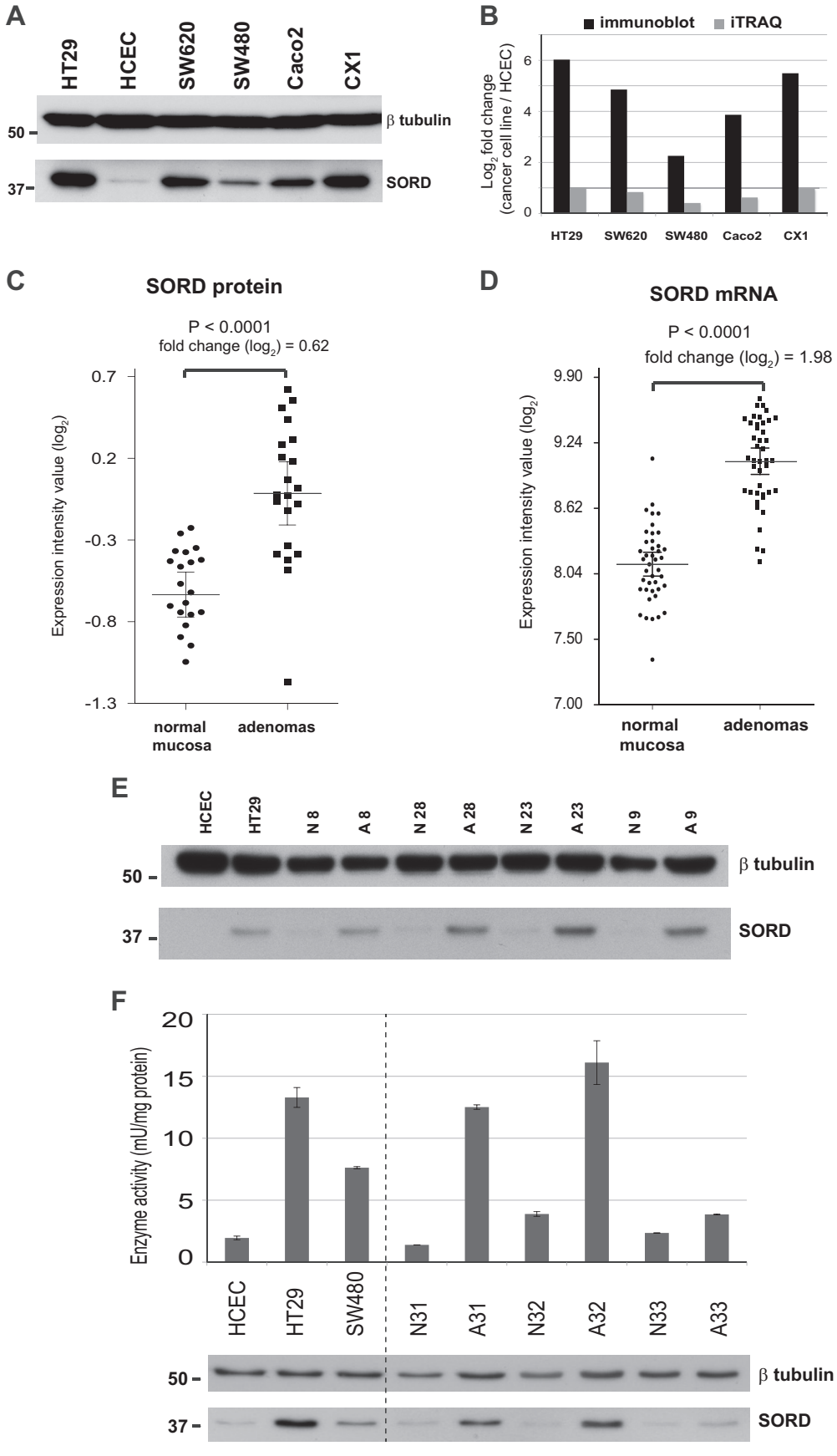
A
HT29
HCEC
SW620
SW480
Caco2
CX1
50
β tubulin
37
SORD
B
immunoblot
iTRAQ
Log2 fold change (cancer cell line / HCEC)
0
2
4
6
HT29
SW620
SW480
Caco2
CX1
C
SORD protein
P < 0.0001
fold change (log2) = 0.62
Expression intensity value (log2)
0.7
0.2
-0.3
-0.8
-1.3
normal mucosa
adenomas
D
SORD mRNA
P < 0.0001
fold change (log2) = 1.98
Expression intensity value (log2)
9.90
9.24
8.62
8.04
7.50
7.00
normal mucosa
adenomas
E
HCEC
HT29
N 8
A 8
N 28
A 28
N 23
A 23
N 9
A 9
50
β tubulin
37
SORD
F
Enzyme activity (mU/mg protein)
0
5
10
15
20
HCEC
HT29
SW480
N31
A31
N32
A32
N33
A33
50
β tubulin
37
SORD

of stromal-cell origin, as they were not expressed in any of the six epithelial cell lines we examined (Table III). These proteins were mainly involved in immune-related processes (immune response, complement activation, T-cell co-stimulation), which are usually not represented in colon epithelial cell lines. Their expression changes are likely to have important effects on the microenvironment of an epithelial-cell tumor.

Our search for potential biomarkers of early-stage colorectal tumorigenesis focused exclusively on the 76 proteins whose expression was significantly up-regulated in adenomas. According to the Human Protein Atlas database (36), 69 (91%) of these have cancer-related features, and 16 of the 69 are already classified as candidate cancer biomarkers (Table III). The Human Protein Atlas database contains information on protein expression in normal and cancer tissues, but not in those regarded as precancerous. The overlap between our findings and those of the Human Protein Atlas suggest that most protein expression changes identified thus far in colorectal adenocarcinomas are probably already detectable in the benign precursors of these lesions. Supplemental Fig. S6 shows the expression profiles of the 10 proteins that were most markedly up-regulated in adenomas. This group included two of the four proteins identified by Lam *et al.* (35) as significantly overexpressed in adenomas. Annexin A3 (ANXA3), for example, is at the top of our list (based on q values) (Table III). An angiogenic factor that induces VEGF production via the HIF-1 pathway (37), ANXA3 belongs to a family of calcium-dependent, phospholipid-binding proteins involved in diverse biological processes, including signal transduction, inflammatory responses, membrane organization, and the regulation of cellular growth (38, 39). Dysregulated ANXA expression is also a common feature of colorectal cancer (39), and most other cancers as well (40). S100A11 expression was also increased in these tumors, which is consistent with earlier reports (41). The cytosolic S100 proteins interact directly with peptides on the N-terminal domain of annexins (38, 42), and like the annexins, they also have diverse intracellular and extracellular functional roles (43).

Among the other top 10 proteins displaying adenoma-related up-regulation were LDHA and LDHB. Their expression levels were not measured separately, but LDHA is presumably responsible for the increased expression observed in our adenomas. *LDHB* expression is in most cases epigenetically silenced in colon cancer cells (44, 45), whereas *LDHA* is overexpressed, and its activity is maintained via the oncogenic tyrosine kinase FGFR1 (46). LDHA is a key player in the reversible conversion of pyruvate to lactate during aerobic glycolysis, a typical feature of cancer cell metabolism first described by Warburg (47). The sodium- and potassium-coupled chloride cotransporter SLC12A2 is expressed on the basolateral membrane of the normal colon epithelium, where its recruitment and activation are regulated by calcium and cAMP. Loss of SLC12A2 leads to impaired chloride secretion in the intestine (48, 49), but to our knowledge, there are no published data linking this protein to colon cancer. The fifth markedly overexpressed protein was SET, one of the five proteins that make up the inhibitor of acetyltranferases (INHAT) complex. Two other INHAT components, APEX1 and ANP32A/ANP32B, were also up-regulated in adenomas (albeit to a lesser extent than SET) (Table III). These changes are noteworthy because INHAT binds directly to histones, preventing their acetylation by histone acetyl transferases (50–52), and loss of histone acetylation is a crucial step in gene silencing (53, 54). Thus far, INHAT's role in cancer has not been widely investigated, but overexpression of the complex components has been observed in serous epithelial ovarian cancer (55). The up-regulated expression of PPA1/PPA2 in our adenomas might play various roles in colorectal tumorigenesis, as these proteins are key players in the synthesis of fatty acids, nucleotides, amino acids, and other essential molecules (56). The phosphoprotein nucleolin, an essential protein for proliferating cells (57), appears to regulate several steps in the biogenesis of ribosomes, including transcription, ribosome assembly, and the processing of precursor ribosomal RNA (58–60), all of which might be instrumental in adenoma growth. As for OCIAD2, strong immunoreactivity for this protein has been reported in early-stage adenocarcinomas of the lung and in ovarian cancers (61–63), but there are no published data linking it to colorectal tumorigenesis. In contrast, the secreted protein REG4, which promotes mitosis and enhances the motility and invasiveness of colon cancer cells, is strongly expressed in these cells and in the serum of patients with colorectal cancer (64–66).

The final protein characterized by marked adenoma-related up-regulation was SORD, a key enzyme in the polyol metabolic pathway. It was selected for validation studies because although aberrant polyol pathway activity has been implicated in diabetic complications (67–70) and myocardial ischemia

FIG. 5. **Significantly up-regulated SORD expression and activity in colorectal cell lines and adenomas.** *A*, tumor-related up-regulation of sorbitol dehydrogenase (SORD) in colon cancer cell lines was confirmed with Western blotting. The SORD dysregulation trend was identical to that observed with iTRAQ-based MS/MS, although when immunoblot results were quantified (*B*), the $\log_2$ fold changes were more than five times greater than those documented in the iTRAQ study. *C*, SORD protein expression (iTRAQ analysis) in 21 normal mucosa–adenoma tissue pairs. *D*, *SORD* mRNA expression in 42 other normal mucosa–adenoma pairs from a previous study by our group (26). Error bars indicate the means and 95% confidence intervals. *E*, Western blots showing tumor-related up-regulation of SORD expression in four randomly selected adenoma (A)/normal mucosa (N) tissue pairs of the 21 shown in panel *C* (see Table I for sample descriptions). *F*, SORD activity also displayed tumor-related up-regulation in cell lines (HT29 and SW480 *versus* HCEC cells) and tissues (adenomas *versus* normal mucosa). Columns show mean enzyme activity measured in at least two replicates; error bars indicate standard deviations from means. The Western blot beneath the graph shows SORD levels measured in the extracts used for the enzyme activity assays.

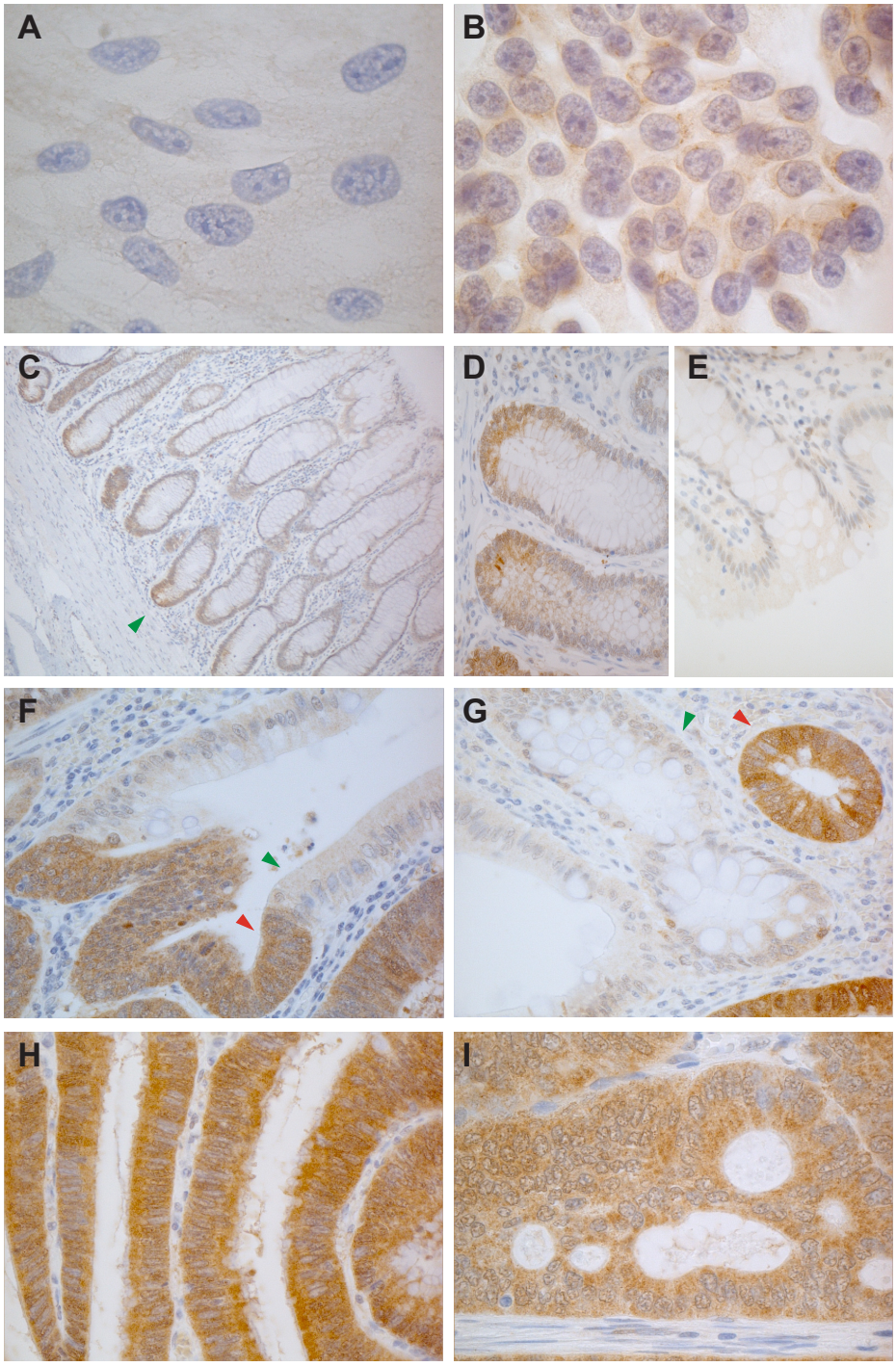

FIG. 6. **Anti-SORD immunostaining of colorectal cell lines and tissues.** Consistent with proteomic data, SORD expression was (*A*) negligible or absent in HCECs but (*B*) clearly expressed in the cytoplasm of HT29 cells. *C*, in normal colorectal mucosa, SORD expression was limited to the lower portion of the epithelial crypts, where stem cells and highly proliferating cells are located. Higher magnification views show staining at (*D*) the base *versus* (*E*) the mouth of colonic crypts. *F*, *G*, its expression was markedly increased in adenomatous glands (red arrowheads) relative to normal crypts (green arrowheads). Panels *H* and *I* show abundant expression of SORD in a large adenoma and in a cancer, respectively.

(71), the role of SORD in tumorigenesis was completely unknown. During the execution of this study, however, up-regulated SORD expression was reported in prostate cancer (72) and in colorectal adenomas (21), and these findings strengthened our resolve to characterize this phenomenon in colorectal tumorigenesis.

Up-regulated SORD expression and activity in adenomas (Fig. 5) would enhance the production of fructose (see sche-

matic of supplemental Fig. S5*A*), thereby increasing the generation of triose sugars and diacylglycerol (intermediates in the glycolytic and lipid signaling pathways, respectively). Fructose is also several times more effective than glucose in promoting intracellular non-enzymatic glycation (73–75), and advanced glycation end products may contribute to the vascular complications of diabetes and other pathologic conditions (67, 76–78). Whether these fructose-driven metabolic events play a role in the development of adenomas is unclear, but the polyol pathway was very active in the adenomatous cells we examined. This activity was also reflected in the concomitant increase of the expression of KHK (supplemental Fig. S5*B*), the enzyme that catalyzes the transformation of fructose to fructose-1-P, downstream from the polyol pathway.

The effects of these enzymatic changes on sorbitol and fructose concentrations in adenomas need to be investigated in larger tissue series, but our preliminary data suggest that the levels of both are slightly decreased in these lesions (supplemental Fig. S5*C*). In contrast, our adenomas exhibited dramatically reduced concentrations of glucose, the initial substrate in the polyol pathway (supplemental Fig. S5*C*). Adenoma-related dysregulation was also noted in the expression of AKR1B1, the enzyme that converts glucose to sorbitol (supplemental Fig. S5*B*). Exploitation of the polyol pathway to divert carbon from glucose to other energy intermediates might provide adenomatous cells with a selective advantage over normal cells. This pathway might prove to be another means of tumor-related glucose consumption in addition to the well-known glycolytic and pentose phosphate pathways (supplemental Fig. S5*A*). Advanced cancer cells consume glucose at a much higher rate than normal cells, and much of their energy is generated by aerobic glycolysis rather than by oxidative phosphorylation of glucose in the mitochondria (*i.e.* the Warburg effect) (79). The predominantly glycolytic phenotype of cancer cells results in low glucose levels and high concentrations of lactate (47, 80, 81). The relative concentrations of lactate in the three adenomas we tested were significantly greater than those found in matched samples of normal mucosa (supplemental Fig. S5*C*), indicating that the Warburg effect is already evident in precancerous colorectal lesions. Studies involving metabolic flux analysis to monitor the fate of isotopic tracers in *in vitro* and *in vivo* systems would provide further insight into the biological roles of the polyol pathway in tumorigenesis. Further information on selected PSMs, peptides, and corresponding assembled proteins can be found in supplemental Tables S1 (tissues) and S3 (cell lines). Supplemental Figs. S7 through S17 show spectra for the proteins identified with a single peptide (listed in supplemental Tables S1 and S3).

Acknowledgments—We thank Ritva Haider, Mirjam Schneider, Asa Wahlander, Bernd Roschitzki, Claudia Fortes, Tshering Altherr, Michal J. Okoniewski, and Katrin Hecht for technical assistance; Paola Picotti, Bernd Wollscheid, Joseph Jiricny, Javier Pena Diaz, Mirco Menigatti, and David Fischer for productive discussion; and Marian Everett Kent for editing the manuscript. The MS data have been deposited in the ProteomeXchange Consortium (http://proteomecentral.proteomexchange.org) via the PRIDE partner repository with the dataset identifier PXD000445 and DOI 10.6019/PXD000445.

* The research was supported by a grant from the Swiss National Science Foundation (Grant No. 31003A_141225).

S This article contains supplemental material.

** To whom correspondence should be addressed: Giancarlo Marra, M.D., Ph.D., Institute of Molecular Cancer Research, University of Zurich, Winterthurerstrasse 190, 8057 Zurich, Switzerland; Tel.: 0041-44-635-3472; Fax: 0041-44-635-3484; E-mail: marra@imcr.uzh.ch.

REFERENCES

1. Jemal, A., Bray, F., Center, M. M., Ferlay, J., Ward, E., and Forman, D. (2011) Global cancer statistics. *CA Cancer J. Clin.* **61,** 69–90
2. Siegel, R., Naishadham, D., and Jemal, A. (2013) Cancer statistics, 2013. *CA Cancer J. Clin.* **63,** 11–30
3. Shinya, H., and Wolff, W. I. (1979) Morphology, anatomic distribution and cancer potential of colonic polyps. *Ann. Surg.* **190,** 679–683
4. Cattaneo, E., Baudis, M., Buffoli, F., Bianco, M. A., Zorzi, F., and Marra, G. (2011) Pathways and crossroads to colorectal cancer In *Pre-Invasive Disease: Pathogenesis and Clinical Management* (Fitzgerald, R. C., ed), pp. 369–394, Springer, New York
5. U.S. Multi-Society Task Force (2002) Screening for colorectal cancer: recommendation and rationale. *Ann. Intern. Med.* **137,** 129–131
6. Kahi, C. J., Rex, D. K., and Imperiale, T. F. (2008) Screening, surveillance, and primary prevention for colorectal cancer: a review of the recent literature. *Gastroenterology* **135,** 380–399
7. Levin, B., Lieberman, D. A., McFarland, B., Andrews, K. S., Brooks, D., Bond, J., Dash, C., Giardiello, F. M., Glick, S., Johnson, D., Johnson, C. D., Levin, T. R., Pickhardt, P. J., Rex, D. K., Smith, R. A., Thorson, A., Winawer, S. J., American Cancer Society Colorectal Cancer Advisory, U.S. Multi-Society Task Force, and American College of Radiology Colon Cancer (2008) Screening and surveillance for the early detection of colorectal cancer and adenomatous polyps, 2008: a joint guideline from the American Cancer Society, the US Multi-Society Task Force on Colorectal Cancer, and the American College of Radiology. *Gastroenterology* **134,** 1570–1595
8. Sillars-Hardebol, A. H., Carvalho, B., van Engeland, M., Fijneman, R. J., and Meijer, G. A. (2012) The adenoma hunt in colorectal cancer screening: defining the target. *J. Pathol.* **226,** 1–6
9. de Wit, M., Fijneman, R. J., Verheul, H. M., Meijer, G. A., and Jimenez, C. R. (2013) Proteomics in colorectal cancer translational research: biomarker discovery for clinical applications. *Clin. Biochem.* **46,** 466–479
10. Patterson, S. D., and Aebersold, R. H. (2003) Proteomics: the first decade and beyond. *Nat. Genet.* **33 Suppl,** 311–323
11. Horth, P., Miller, C. A., Preckel, T., and Wenz, C. (2006) Efficient fractionation and improved protein identification by peptide OFFGEL electrophoresis. *Mol. Cell. Proteomics* **5,** 1968–1974
12. Wu, W. W., Wang, G., Baek, S. J., and Shen, R. F. (2006) Comparative study of three proteomic quantitative methods, DIGE, cICAT, and iTRAQ, using 2D gel or LC-MALDI TOF/TOF. *J. Proteome Res.* **5,** 651–658
13. Aebersold, R., and Mann, M. (2003) Mass spectrometry-based proteomics. *Nature* **422,** 198–207
14. Aebersold, R., and Goodlett, D. R. (2001) Mass spectrometry in proteomics. *Chem. Rev.* **101,** 269–295
15. Bensimon, A., Heck, A. J., and Aebersold, R. (2012) Mass spectrometry-based proteomics and network biology. *Annu. Rev. Biochem.* **81,** 379–405
16. Bantscheff, M., Lemeer, S., Savitski, M. M., and Kuster, B. (2012) Quantitative mass spectrometry in proteomics: critical review update from 2007 to the present. *Anal. Bioanal. Chem.* **404,** 939–965
17. Wiese, S., Reidegeld, K. A., Meyer, H. E., and Warscheid, B. (2007) Protein labeling by iTRAQ: a new tool for quantitative mass spectrometry in proteome research. *Proteomics* **7,** 340–350
18. Gan, C. S., Chong, P. K., Pham, T. K., and Wright, P. C. (2007) Technical, experimental, and biological variations in isobaric tags for relative and absolute quantitation (iTRAQ). *J. Proteome Res.* **6,** 821–827

19. Ross, P. L., Huang, Y. N., Marchese, J. N., Williamson, B., Parker, K., Hattan, S., Khainovski, N., Pillai, S., Dey, S., Daniels, S., Purkayastha, S., Juhasz, P., Martin, S., Bartlet-Jones, M., He, F., Jacobson, A., and Pappin, D. J. (2004) Multiplexed protein quantitation in Saccharomyces cerevisiae using amine-reactive isobaric tagging reagents. *Mol. Cell. Proteomics* **3,** 1154–1169
20. Jimenez, C. R., Knol, J. C., Meijer, G. A., and Fijneman, R. J. (2010) Proteomics of colorectal cancer: overview of discovery studies and identification of commonly identified cancer-associated proteins and candidate CRC serum markers. *J. Proteomics* **73,** 1873–1895
21. Besson, D., Pavageau, A. H., Valo, I., Bourreau, A., Belanger, A., Eymerit-Morin, C., Mouliere, A., Chassevent, A., Boisdron-Celle, M., Morel, A., Solassol, J., Campone, M., Gamelin, E., Barre, B., Coqueret, O., and Guette, C. (2011) A quantitative proteomic approach of the different stages of colorectal cancer establishes OLFM4 as a new nonmetastatic tumor marker. *Mol. Cell. Proteomics* **10,** M111.009712
22. Jankova, L., Chan, C., Fung, C. L., Song, X., Kwun, S. Y., Cowley, M. J., Kaplan, W., Dent, O. F., Bokey, E. L., Chapuis, P. H., Baker, M. S., Robertson, G. R., Clarke, S. J., and Molloy, M. P. (2011) Proteomic comparison of colorectal tumours and non-neoplastic mucosa from paired patient samples using iTRAQ mass spectrometry. *Mol. Biosyst.* **7,** 2997–3005
23. Roig, A. I., Eskiocak, U., Hight, S. K., Kim, S. B., Delgado, O., Souza, R. F., Spechler, S. J., Wright, W. E., and Shay, J. W. (2010) Immortalized epithelial cells derived from human colon biopsies express stem cell markers and differentiate in vitro. *Gastroenterology* **138,** 1012–1021
24. Kall, L., Storey, J. D., MacCoss, M. J., and Noble, W. S. (2008) Posterior error probabilities and false discovery rates: two sides of the same coin. *J. Proteome Res.* **7,** 40–44
25. Alexa, A., Rahnenfuhrer, J., and Lengauer, T. (2006) Improved scoring of functional groups from gene expression data by decorrelating GO graph structure. *Bioinformatics* **22,** 1600–1607
26. Cattaneo, E., Laczko, E., Buffoli, F., Zorzi, F., Bianco, M. A., Menigatti, M., Bartosova, Z., Haider, R., Helmchen, B., Sabates-Bellver, J., Tiwari, A., Jiricny, J., and Marra, G. (2011) Preinvasive colorectal lesion transcriptomes correlate with endoscopic morphology (polypoid vs. nonpolypoid). *EMBO Mol. Med.* **3,** 334–347
27. Truninger, K., Menigatti, M., Luz, J., Russell, A., Haider, R., Gebbers, J. O., Bannwart, F., Yurtsever, H., Neuweiler, J., Riehle, H. M., Cattaruzza, M. S., Heinimann, K., Schär, P., Jiricny, J., and Marra, G. (2005) Immunohistochemical analysis reveals high frequency of PMS2 defects in colorectal cancer. *Gastroenterology* **128,** 1160–1171
28. Gerlach, U., and Hilby, W. (1974) *Methods of Enzymatic Analysis*, 2nd Ed., Academic Press Inc., New York
29. Lisec, J., Schauer, N., Kopka, J., Willmitzer, L., and Fernie, A. R. (2006) Gas chromatography mass spectrometry-based metabolite profiling in plants. *Nat. Protoc.* **1,** 387–396
30. Afkarian, M., Bhasin, M., Dillon, S. T., Guerrero, M. C., Nelson, R. G., Knowler, W. C., Thadhani, R., and Libermann, T. A. (2010) Optimizing a proteomics platform for urine biomarker discovery. *Mol. Cell. Proteomics* **9,** 2195–2204
31. Ishihama, Y., Oda, Y., Tabata, T., Sato, T., Nagasu, T., Rappsilber, J., and Mann, M. (2005) Exponentially modified protein abundance index (emPAI) for estimation of absolute protein amount in proteomics by the number of sequenced peptides per protein. *Mol. Cell. Proteomics* **4,** 1265–1272
32. Maglietta, R., Liuzzi, V. C., Cattaneo, E., Laczko, E., Piepoli, A., Panza, A., Carella, M., Palumbo, O., Staiano, T., Buffoli, F., Andriulli, A., Marra, G., and Ancona, N. (2012) Molecular pathways undergoing dramatic transcriptomic changes during tumor development in the human colon. *BMC Cancer* **12,** 608
33. Ow, S. Y., Salim, M., Noirel, J., Evans, C., Rehman, I., and Wright, P. C. (2009) iTRAQ underestimation in simple and complex mixtures: "the good, the bad and the ugly." *J. Proteome Res.* **8,** 5347–5355
34. Albrethsen, J., Knol, J. C., Piersma, S. R., Pham, T. V., de Wit, M., Mongera, S., Carvalho, B., Verheul, H. M., Fijneman, R. J., Meijer, G. A., and Jimenez, C. R. (2010) Subnuclear proteomics in colorectal cancer: identification of proteins enriched in the nuclear matrix fraction and regulation in adenoma to carcinoma progression. *Mol. Cell. Proteomics* **9,** 988–1005
35. Lam, F., Jankova, L., Dent, O. F., Molloy, M. P., Kwun, S. Y., Clarke, C., Chapuis, P., Robertson, G., Beale, P., Clarke, S., Bokey, E. L., and Chan, C. (2010) Identification of distinctive protein expression patterns in colorectal adenoma. *Proteomics Clin. Appl.* **4,** 60–70
36. Uhlen, M., Oksvold, P., Fagerberg, L., Lundberg, E., Jonasson, K., Forsberg, M., Zwahlen, M., Kampf, C., Wester, K., Hober, S., Wernerus, H., Bjorling, L., and Ponten, F. (2010) Towards a knowledge-based Human Protein Atlas. *Nat. Biotechnol.* **28,** 1248–1250
37. Park, J. E., Lee, D. H., Lee, J. A., Park, S. G., Kim, N. S., Park, B. C., and Cho, S. (2005) Annexin A3 is a potential angiogenic mediator. *Biochem. Biophys. Res. Commun.* **337,** 1283–1287
38. Gerke, V., Creutz, C. E., and Moss, S. E. (2005) Annexins: linking Ca2+ signalling to membrane dynamics. *Nat. Rev. Mol. Cell Biol.* **6,** 449–461
39. Duncan, R., Carpenter, B., Main, L. C., Telfer, C., and Murray, G. I. (2008) Characterisation and protein expression profiling of annexins in colorectal cancer. *Br. J. Cancer* **98,** 426–433
40. Mussunoor, S., and Murray, G. I. (2008) The role of annexins in tumour development and progression. *J. Pathol.* **216,** 131–140
41. Melle, C., Ernst, G., Schimmel, B., Bleul, A., Mothes, H., Kaufmann, R., Settmacher, U., and Von Eggeling, F. (2006) Different expression of calgizzarin (S100A11) in normal colonic epithelium, adenoma and colorectal carcinoma. *Int. J. Oncol.* **28,** 195–200
42. Lewit-Bentley, A., Rety, S., Sopkova-de Oliveira Santos, J., and Gerke, V. (2000) S100-annexin complexes: some insights from structural studies. *Cell Biol. Int.* **24,** 799–802
43. Donato, R. (2001) S100: a multigenic family of calcium-modulated proteins of the EF-hand type with intracellular and extracellular functional roles. *Int. J. Biochem. Cell Biol.* **33,** 637–668
44. Thangaraju, M., Carswell, K. N., Prasad, P. D., and Ganapathy, V. (2009) Colon cancer cells maintain low levels of pyruvate to avoid cell death caused by inhibition of HDAC1/HDAC3. *Biochem. J.* **417,** 379–389
45. Thorn, C. C., Freeman, T. C., Scott, N., Guillou, P. J., and Jayne, D. G. (2009) Laser microdissection expression profiling of marginal edges of colorectal tumours reveals evidence of increased lactate metabolism in the aggressive phenotype. *Gut* **58,** 404–412
46. Fan, J., Hitosugi, T., Chung, T. W., Xie, J., Ge, Q., Gu, T. L., Polakiewicz, R. D., Chen, G. Z., Boggon, T. J., Lonial, S., Khuri, F. R., Kang, S., and Chen, J. (2011) Tyrosine phosphorylation of lactate dehydrogenase A is important for NADH/NAD(+) redox homeostasis in cancer cells. *Mol. Cell. Biol.* **31,** 4938–4950
47. Koppenol, W. H., Bounds, P. L., and Dang, C. V. (2011) Otto Warburg's contributions to current concepts of cancer metabolism. *Nat. Rev. Cancer* **11,** 325–337
48. Reynolds, A., Parris, A., Evans, L. A., Lindqvist, S., Sharp, P., Lewis, M., Tighe, R., and Williams, M. R. (2007) Dynamic and differential regulation of NKCC1 by calcium and cAMP in the native human colonic epithelium. *J. Physiol.* **582,** 507–524
49. Flagella, M., Clarke, L. L., Miller, M. L., Erway, L. C., Giannella, R. A., Andringa, A., Gawenis, L. R., Kramer, J., Duffy, J. J., Doetschman, T., Lorenz, J. N., Yamoah, E. N., Cardell, E. L., and Shull, G. E. (1999) Mice lacking the basolateral Na-K-2Cl cotransporter have impaired epithelial chloride secretion and are profoundly deaf. *J. Biol. Chem.* **274,** 26946–26955
50. Schneider, R., Bannister, A. J., Weise, C., and Kouzarides, T. (2004) Direct binding of INHAT to H3 tails disrupted by modifications. *J. Biol. Chem.* **279,** 23859–23862
51. Kutney, S. N., Hong, R., Macfarlan, T., and Chakravarti, D. (2004) A signaling role of histone-binding proteins and INHAT subunits pp32 and Set/TAF-Ibeta in integrating chromatin hypoacetylation and transcriptional repression. *J. Biol. Chem.* **279,** 30850–30855
52. Seo, S. B., McNamara, P., Heo, S., Turner, A., Lane, W. S., and Chakravarti, D. (2001) Regulation of histone acetylation and transcription by INHAT, a human cellular complex containing the set oncoprotein. *Cell* **104,** 119–130
53. Kondo, Y., and Issa, J. P. (2004) Epigenetic changes in colorectal cancer. *Cancer Metastasis Rev.* **23,** 29–39
54. Kondo, Y., Shen, L., and Issa, J. P. (2003) Critical role of histone methylation in tumor suppressor gene silencing in colorectal cancer. *Mol. Cell. Biol.* **23,** 206–215
55. Ouellet, V., Le Page, C., Guyot, M. C., Lussier, C., Tonin, P. N., Provencher, D. M., and Mes-Masson, A. M. (2006) SET complex in serous epithelial ovarian cancer. *Int. J. Cancer* **119,** 2119–2126

56. Takahashi, K., Inuzuka, M., and Ingi, T. (2004) Cellular signaling mediated by calphoglin-induced activation of IPP and PGM. *Biochem. Biophys. Res. Commun.* **325,** 203–214
57. Lapeyre, B., Bourbon, H., and Amalric, F. (1987) Nucleolin, the major nucleolar protein of growing eukaryotic cells: an unusual protein structure revealed by the nucleotide sequence. *Proc. Natl. Acad. Sci. U.S.A.* **84,** 1472–1476
58. Ginisty, H., Amalric, F., and Bouvet, P. (1998) Nucleolin functions in the first step of ribosomal RNA processing. *EMBO J.* **17,** 1476–1486
59. Ginisty, H., Sicard, H., Roger, B., and Bouvet, P. (1999) Structure and functions of nucleolin. *J. Cell Sci.* **112 (Pt 6),** 761–772
60. Tajrishi, M. M., Tuteja, R., and Tuteja, N. (2011) Nucleolin: the most abundant multifunctional phosphoprotein of nucleolus. *Commun. Integr. Biol.* **4,** 267–275
61. Chien, J., Fan, J. B., Bell, D. A., April, C., Klotzle, B., Ota, T., Lingle, W. L., Gonzalez Bosquet, J., Shridhar, V., and Hartmann, L. C. (2009) Analysis of gene expression in stage I serous tumors identifies critical pathways altered in ovarian cancer. *Gynecol. Oncol.* **114,** 3–11
62. Ishiyama, T., Kano, J., Anami, Y., Onuki, T., Iijima, T., Morisita, Y., Yokota, J., and Noguchi, M. (2007) OCIA domain containing 2 is highly expressed in adenocarcinoma mixed subtype with bronchioloalveolar carcinoma component and is associated with better prognosis. *Cancer Sci.* **98,** 50–57
63. Nagata, C., Kobayashi, H., Sakata, A., Satomi, K., Minami, Y., Morishita, Y., Ohara, R., Yoshikawa, H., Arai, Y., Nishida, M., and Noguchi, M. (2012) Increased expression of OCIA domain containing 2 during stepwise progression of ovarian mucinous tumor. *Pathol. Int.* **62,** 471–476
64. Oue, N., Kuniyasu, H., Noguchi, T., Sentani, K., Ito, M., Tanaka, S., Setoyama, T., Sakakura, C., Natsugoe, S., and Yasui, W. (2007) Serum concentration of Reg IV in patients with colorectal cancer: overexpression and high serum levels of Reg IV are associated with liver metastasis. *Oncology* **72,** 371–380
65. Rafa, L., Dessein, A. F., Devisme, L., Buob, D., Truant, S., Porchet, N., Huet, G., Buisine, M. P., and Lesuffleur, T. (2010) REG4 acts as a mitogenic, motility and pro-invasive factor for colon cancer cells. *Int. J. Oncol.* **36,** 689–698
66. Violette, S., Festor, E., Pandrea-Vasile, I., Mitchell, V., Adida, C., Dussaulx, E., Lacorte, J. M., Chambaz, J., Lacasa, M., and Lesuffleur, T. (2003) Reg IV, a new member of the regenerating gene family, is overexpressed in colorectal carcinomas. *Int. J. Cancer* **103,** 185–193
67. Obrosova, I. G. (2005) Increased sorbitol pathway activity generates oxidative stress in tissue sites for diabetic complications. *Antioxid. Redox Signal.* **7,** 1543–1552
68. Ola, M. S., Berkich, D. A., Xu, Y., King, M. T., Gardner, T. W., Simpson, I., and LaNoue, K. F. (2006) Analysis of glucose metabolism in diabetic rat retinas. *Am. J. Physiol. Endocrinol. Metab.* **290,** E1057-E1067
69. Van den Enden, M. K., Nyengaard, J. R., Ostrow, E., Burgan, J. H., and Williamson, J. R. (1995) Elevated glucose levels increase retinal glycolysis and sorbitol pathway metabolism. Implications for diabetic retinopathy. *Invest. Ophthalmol. Vis. Sci.* **36,** 1675–1685
70. Gabbay, K. H., Merola, L. O., and Field, R. A. (1966) Sorbitol pathway: presence in nerve and cord with substrate accumulation in diabetes. *Science* **151,** 209–210
71. Hwang, Y. C., Bakr, S., Ellery, C. A., Oates, P. J., and Ramasamy, R. (2003) Sorbitol dehydrogenase: a novel target for adjunctive protection of ischemic myocardium. *FASEB J.* **17,** 2331–2333
72. Szabo, Z., Hamalainen, J., Loikkanen, I., Moilanen, A. M., Hirvikoski, P., Vaisanen, T., Paavonen, T. K., and Vaarala, M. H. (2010) Sorbitol dehydrogenase expression is regulated by androgens in the human prostate. *Oncol. Rep.* **23,** 1233–1239
73. Obrosova, I. G. (2005) Increased sorbitol pathway activity generates oxidative stress in tissue sites for diabetic complications. *Antioxid. Redox Signal.* **7,** 1543–1552
74. Dills, W. L., Jr. (1993) Protein fructosylation: fructose and the Maillard reaction. *Am. J. Clin. Nutr.* **58,** 779S-787S
75. Suarez, G., Rajaram, R., Oronsky, A. L., and Gawinowicz, M. A. (1989) Nonenzymatic glycation of bovine serum albumin by fructose (fructation). Comparison with the Maillard reaction initiated by glucose. *J. Biol. Chem.* **264,** 3674–3679
76. Schalkwijk, C. G., Stehouwer, C. D., and van Hinsbergh, V. W. (2004) Fructose-mediated non-enzymatic glycation: sweet coupling or bad modification. *Diabetes Metab. Res. Rev.* **20,** 369–382
77. Bose, T., and Chakraborti, A. S. (2008) Fructose-induced structural and functional modifications of hemoglobin: implication for oxidative stress in diabetes mellitus. *Biochim. Biophys. Acta* **1780,** 800–808
78. Schmidt, A. M., Hori, O., Brett, J., Yan, S. D., Wautier, J. L., and Stern, D. (1994) Cellular receptors for advanced glycation end products. Implications for induction of oxidant stress and cellular dysfunction in the pathogenesis of vascular lesions. *Arterioscler. Thromb.* **14,** 1521–1528
79. Warburg, O. (1956) On the origin of cancer cells. *Science* **123,** 309–314
80. Chan, E. C., Koh, P. K., Mal, M., Cheah, P. Y., Eu, K. W., Backshall, A., Cavill, R., Nicholson, J. K., and Keun, H. C. (2009) Metabolic profiling of human colorectal cancer using high-resolution magic angle spinning nuclear magnetic resonance (HR-MAS NMR) spectroscopy and gas chromatography mass spectrometry (GC/MS). *J. Proteome Res.* **8,** 352–361
81. Hirayama, A., Kami, K., Sugimoto, M., Sugawara, M., Toki, N., Onozuka, H., Kinoshita, T., Saito, N., Ochiai, A., Tomita, M., Esumi, H., and Soga, T. (2009) Quantitative metabolome profiling of colon and stomach cancer microenvironment by capillary electrophoresis time-of-flight mass spectrometry. *Cancer Res.* **69,** 4918–4925
82. Kudo, S., Rubio, C. A., Teixeira, C. R., Kashida, H., Kogure, E. et al. (2001) Pit pattern in colorectal neoplasia: endoscopic magnifying view. *Endoscopy* **33,** 367